DESY-08-177

Measurement of charged current deep inelastic scattering cross sections with a longitudinally polarised electron beam at HERA

ZEUS Collaboration

Abstract

Measurements of the cross sections for charged current deep inelastic scattering in $e^- p$ collisions with longitudinally polarised electron beams are presented. The measurements are based on a data sample with an integrated luminosity of $175\,\mathrm{pb}^{-1}$ collected with the ZEUS detector at HERA at a centre-of-mass energy of 318 GeV. The total cross section is given for positively and negatively polarised electron beams. The differential cross-sections $d\sigma/dQ^2$, $d\sigma/dx$ and $d\sigma/dy$ are presented for $Q^2 > 200\,\mathrm{GeV}^2$. The double-differential cross-section $d^2\sigma/dxdQ^2$ is presented in the kinematic range $280 < Q^2 < 30\,000\,\mathrm{GeV}^2$ and $0.015 < x < 0.65$. The measured cross sections are compared with the predictions of the Standard Model.

The ZEUS Collaboration

S. Chekanov, M. Derrick, S. Magill, B. Musgrave, D. Nicholass[1], J. Repond, R. Yoshida
Argonne National Laboratory, Argonne, Illinois 60439-4815, USA [n]

M.C.K. Mattingly
Andrews University, Berrien Springs, Michigan 49104-0380, USA

P. Antonioli, G. Bari, L. Bellagamba, D. Boscherini, A. Bruni, G. Bruni, F. Cindolo, M. Corradi, G. Iacobucci, A. Margotti, R. Nania, A. Polini
INFN Bologna, Bologna, Italy [e]

S. Antonelli, M. Basile, M. Bindi, L. Cifarelli, A. Contin, S. De Pasquale[2], G. Sartorelli, A. Zichichi
University and INFN Bologna, Bologna, Italy [e]

D. Bartsch, I. Brock, H. Hartmann, E. Hilger, H.-P. Jakob, M. Jüngst, A.E. Nuncio-Quiroz, E. Paul, U. Samson, V. Schönberg, R. Shehzadi, M. Wlasenko
Physikalisches Institut der Universität Bonn, Bonn, Germany [b]

N.H. Brook, G.P. Heath, J.D. Morris
H.H. Wills Physics Laboratory, University of Bristol, Bristol, United Kingdom [m]

M. Kaur, P. Kaur[3], I. Singh[3]
Panjab University, Department of Physics, Chandigarh, India

M. Capua, S. Fazio, A. Mastroberardino, M. Schioppa, G. Susinno, E. Tassi
Calabria University, Physics Department and INFN, Cosenza, Italy [e]

J.Y. Kim
Chonnam National University, Kwangju, South Korea

Z.A. Ibrahim, F. Mohamad Idris, B. Kamaluddin, W.A.T. Wan Abdullah
Jabatan Fizik, Universiti Malaya, 50603 Kuala Lumpur, Malaysia [r]

Y. Ning, Z. Ren, F. Sciulli
Nevis Laboratories, Columbia University, Irvington on Hudson, New York 10027 [o]

J. Chwastowski, A. Eskreys, J. Figiel, A. Galas, K. Olkiewicz, B. Pawlik, P. Stopa, L. Zawiejski
The Henryk Niewodniczanski Institute of Nuclear Physics, Polish Academy of Sciences, Cracow, Poland [i]

L. Adamczyk, T. Bołd, I. Grabowska-Bołd, D. Kisielewska, J. Łukasik[4], M. Przybycień, L. Suszycki
Faculty of Physics and Applied Computer Science, AGH-University of Science and Technology, Cracow, Poland [p]

A. Kotański[5], W. Słomiński[6]
Department of Physics, Jagellonian University, Cracow, Poland

O. Behnke, U. Behrens, C. Blohm, A. Bonato, K. Borras, D. Bot, R. Ciesielski, N. Coppola, S. Fang, J. Fourletova[7], A. Geiser, P. Göttlicher[8], J. Grebenyuk, I. Gregor, T. Haas, W. Hain, A. Hüttmann, F. Januschek, B. Kahle, I.I. Katkov[9], U. Klein[10], U. Kötz, H. Kowalski, M. Lisovyi, E. Lobodzinska, B. Löhr, R. Mankel[11], I.-A. Melzer-Pellmann, S. Miglioranzi[12], A. Montanari, T. Namsoo, D. Notz[11], A. Parenti, L. Rinaldi[13], P. Roloff, I. Rubinsky, U. Schneekloth, A. Spiridonov[14], D. Szuba[15], J. Szuba[16], T. Theedt, J. Ukleja[17], G. Wolf, K. Wrona, A.G. Yagües Molina, C. Youngman, W. Zeuner[11]
Deutsches Elektronen-Synchrotron DESY, Hamburg, Germany

V. Drugakov, W. Lohmann, S. Schlenstedt
Deutsches Elektronen-Synchrotron DESY, Zeuthen, Germany

G. Barbagli, E. Gallo
INFN Florence, Florence, Italy [e]

P. G. Pelfer
University and INFN Florence, Florence, Italy [e]

A. Bamberger, D. Dobur, F. Karstens, N.N. Vlasov[18]
Fakultät für Physik der Universität Freiburg i.Br., Freiburg i.Br., Germany [b]

P.J. Bussey[19], A.T. Doyle, W. Dunne, M. Forrest, M. Rosin, D.H. Saxon, I.O. Skillicorn
Department of Physics and Astronomy, University of Glasgow, Glasgow, United Kingdom [m]

I. Gialas[20], K. Papageorgiu
Department of Engineering in Management and Finance, Univ. of Aegean, Greece

U. Holm, R. Klanner, E. Lohrmann, H. Perrey, P. Schleper, T. Schörner-Sadenius, J. Sztuk, H. Stadie, M. Turcato
Hamburg University, Institute of Exp. Physics, Hamburg, Germany [b]

C. Foudas, C. Fry, K.R. Long, A.D. Tapper
Imperial College London, High Energy Nuclear Physics Group, London, United Kingdom [m]

T. Matsumoto, K. Nagano, K. Tokushuku[21], S. Yamada, Y. Yamazaki[22]
Institute of Particle and Nuclear Studies, KEK, Tsukuba, Japan [f]

A.N. Barakbaev, E.G. Boos, N.S. Pokrovskiy, B.O. Zhautykov
Institute of Physics and Technology of Ministry of Education and Science of Kazakhstan, Almaty, Kazakhstan

V. Aushev[23], O. Bachynska, M. Borodin, I. Kadenko, A. Kozulia, V. Libov, D. Lontkovskyi, I. Makarenko, Iu. Sorokin, A. Verbytskyi, O. Volynets
Institute for Nuclear Research, National Academy of Sciences, Kiev and Kiev National University, Kiev, Ukraine

D. Son
Kyungpook National University, Center for High Energy Physics, Daegu, South Korea [g]

J. de Favereau, K. Piotrzkowski
Institut de Physique Nucléaire, Université Catholique de Louvain, Louvain-la-Neuve, Belgium [q]

F. Barreiro, C. Glasman, M. Jimenez, L. Labarga, J. del Peso, E. Ron, M. Soares, J. Terrón, C. Uribe-Estrada, M. Zambrana
Departamento de Física Teórica, Universidad Autónoma de Madrid, Madrid, Spain [l]

F. Corriveau, C. Liu, J. Schwartz, R. Walsh, C. Zhou
Department of Physics, McGill University, Montréal, Québec, Canada H3A 2T8 [a]

T. Tsurugai
Meiji Gakuin University, Faculty of General Education, Yokohama, Japan [f]

A. Antonov, B.A. Dolgoshein, D. Gladkov, V. Sosnovtsev, A. Stifutkin, S. Suchkov
Moscow Engineering Physics Institute, Moscow, Russia [j]

R.K. Dementiev, P.F. Ermolov [†], L.K. Gladilin, Yu.A. Golubkov, L.A. Khein, I.A. Korzhavina, V.A. Kuzmin, B.B. Levchenko[24], O.Yu. Lukina, A.S. Proskuryakov, L.M. Shcheglova, D.S. Zotkin
Moscow State University, Institute of Nuclear Physics, Moscow, Russia [k]

I. Abt, A. Caldwell, D. Kollar, B. Reisert, W.B. Schmidke
Max-Planck-Institut für Physik, München, Germany

G. Grigorescu, A. Keramidas, E. Koffeman, P. Kooijman, A. Pellegrino, H. Tiecke, M. Vázquez[12], L. Wiggers
NIKHEF and University of Amsterdam, Amsterdam, Netherlands [h]

N. Brümmer, B. Bylsma, L.S. Durkin, A. Lee, T.Y. Ling
Physics Department, Ohio State University, Columbus, Ohio 43210 [n]

P.D. Allfrey, M.A. Bell, A.M. Cooper-Sarkar, R.C.E. Devenish, J. Ferrando, B. Foster, C. Gwenlan[25], K. Horton[26], K. Oliver, A. Robertson, R. Walczak
Department of Physics, University of Oxford, Oxford United Kingdom [m]

A. Bertolin, F. Dal Corso, S. Dusini, A. Longhin, L. Stanco
INFN Padova, Padova, Italy [e]

P. Bellan, R. Brugnera, R. Carlin, A. Garfagnini, S. Limentani
Dipartimento di Fisica dell' Università and INFN, Padova, Italy [e]

B.Y. Oh, A. Raval, J.J. Whitmore[27]
Department of Physics, Pennsylvania State University, University Park, Pennsylvania 16802 [o]

Y. Iga
Polytechnic University, Sagamihara, Japan [f]

G. D'Agostini, G. Marini, A. Nigro
Dipartimento di Fisica, Università 'La Sapienza' and INFN, Rome, Italy [e]

J.E. Cole[28], J.C. Hart
Rutherford Appleton Laboratory, Chilton, Didcot, Oxon, United Kingdom [m]

H. Abramowicz[29], R. Ingbir, S. Kananov, A. Levy, A. Stern
Raymond and Beverly Sackler Faculty of Exact Sciences, School of Physics, Tel Aviv University, Tel Aviv, Israel [d]

M. Kuze, J. Maeda
Department of Physics, Tokyo Institute of Technology, Tokyo, Japan [f]

R. Hori, S. Kagawa[30], N. Okazaki, S. Shimizu, T. Tawara
Department of Physics, University of Tokyo, Tokyo, Japan [f]

R. Hamatsu, H. Kaji[31], S. Kitamura[32], O. Ota[33], Y.D. Ri
Tokyo Metropolitan University, Department of Physics, Tokyo, Japan [f]

M. Costa, M.I. Ferrero, V. Monaco, R. Sacchi, V. Sola, A. Solano
Università di Torino and INFN, Torino, Italy [e]

M. Arneodo, M. Ruspa
Università del Piemonte Orientale, Novara, and INFN, Torino, Italy [e]

S. Fourletov[7], J.F. Martin, T.P. Stewart
Department of Physics, University of Toronto, Toronto, Ontario, Canada M5S 1A7 [a]

S.K. Boutle[20], J.M. Butterworth, T.W. Jones, J.H. Loizides, M. Wing[34]
Physics and Astronomy Department, University College London, London, United Kingdom [m]

B. Brzozowska, J. Ciborowski[35], G. Grzelak, P. Kulinski, P. Łużniak[36], J. Malka[36], R.J. Nowak, J.M. Pawlak, W. Perlanski[36], T. Tymieniecka[37], A.F. Żarnecki
Warsaw University, Institute of Experimental Physics, Warsaw, Poland

M. Adamus, P. Plucinski[38], A. Ukleja
Institute for Nuclear Studies, Warsaw, Poland

Y. Eisenberg, D. Hochman, U. Karshon
Department of Particle Physics, Weizmann Institute, Rehovot, Israel [c]

E. Brownson, D.D. Reeder, A.A. Savin, W.H. Smith, H. Wolfe
Department of Physics, University of Wisconsin, Madison, Wisconsin 53706, USA [n]

S. Bhadra, C.D. Catterall, Y. Cui, G. Hartner, S. Menary, U. Noor, J. Standage, J. Whyte
Department of Physics, York University, Ontario, Canada M3J 1P3 [a]

[1] also affiliated with University College London, United Kingdom
[2] now at University of Salerno, Italy
[3] also working at Max Planck Institute, Munich, Germany
[4] now at Institute of Aviation, Warsaw, Poland
[5] supported by the research grant no. 1 P03B 04529 (2005-2008)
[6] This work was supported in part by the Marie Curie Actions Transfer of Knowledge project COCOS (contract MTKD-CT-2004-517186)
[7] now at University of Bonn, Germany
[8] now at DESY group FEB, Hamburg, Germany
[9] also at Moscow State University, Russia
[10] now at University of Liverpool, UK
[11] on leave of absence at CERN, Geneva, Switzerland
[12] now at CERN, Geneva, Switzerland
[13] now at Bologna University, Bologna, Italy
[14] also at Institut of Theoretical and Experimental Physics, Moscow, Russia
[15] also at INP, Cracow, Poland
[16] also at FPACS, AGH-UST, Cracow, Poland
[17] partially supported by Warsaw University, Poland
[18] partly supported by Moscow State University, Russia
[19] Royal Society of Edinburgh, Scottish Executive Support Research Fellow
[20] also affiliated with DESY, Germany
[21] also at University of Tokyo, Japan
[22] now at Kobe University, Japan
[23] supported by DESY, Germany
[24] partly supported by Russian Foundation for Basic Research grant no. 05-02-39028-NSFC-a
[25] STFC Advanced Fellow
[26] nee Korcsak-Gorzo
[27] This material was based on work supported by the National Science Foundation, while working at the Foundation.
[28] now at University of Kansas, Lawrence, USA
[29] also at Max Planck Institute, Munich, Germany, Alexander von Humboldt Research Award
[30] now at KEK, Tsukuba, Japan
[31] now at Nagoya University, Japan
[32] member of Department of Radiological Science, Tokyo Metropolitan University, Japan
[33] now at SunMelx Co. Ltd., Tokyo, Japan
[34] also at Hamburg University, Inst. of Exp. Physics, Alexander von Humboldt Research Award and partially supported by DESY, Hamburg, Germany

[35] also at Łódź University, Poland
[36] member of Łódź University, Poland
[37] also at University of Podlasie, Siedlce, Poland
[38] now at Lund Universtiy, Lund, Sweden
[†] deceased

[a] supported by the Natural Sciences and Engineering Research Council of Canada (NSERC)

[b] supported by the German Federal Ministry for Education and Research (BMBF), under contract numbers 05 HZ6PDA, 05 HZ6GUA, 05 HZ6VFA and 05 HZ4KHA

[c] supported in part by the MINERVA Gesellschaft für Forschung GmbH, the Israel Science Foundation (grant no. 293/02-11.2) and the U.S.-Israel Binational Science Foundation

[d] supported by the Israel Science Foundation

[e] supported by the Italian National Institute for Nuclear Physics (INFN)

[f] supported by the Japanese Ministry of Education, Culture, Sports, Science and Technology (MEXT) and its grants for Scientific Research

[g] supported by the Korean Ministry of Education and Korea Science and Engineering Foundation

[h] supported by the Netherlands Foundation for Research on Matter (FOM)

[i] supported by the Polish State Committee for Scientific Research, project no. DESY/256/2006 - 154/DES/2006/03

[j] partially supported by the German Federal Ministry for Education and Research (BMBF)

[k] supported by RF Presidential grant N 1456.2008.2 for the leading scientific schools and by the Russian Ministry of Education and Science through its grant for Scientific Research on High Energy Physics

[l] supported by the Spanish Ministry of Education and Science through funds provided by CICYT

[m] supported by the Science and Technology Facilities Council, UK

[n] supported by the US Department of Energy

[o] supported by the US National Science Foundation. Any opinion, findings and conclusions or recommendations expressed in this material are those of the authors and do not necessarily reflect the views of the National Science Foundation.

[p] supported by the Polish Ministry of Science and Higher Education as a scientific project (2006-2008)

[q] supported by FNRS and its associated funds (IISN and FRIA) and by an Inter-University Attraction Poles Programme subsidised by the Belgian Federal Science Policy Office

[r] supported by an FRGS grant from the Malaysian government

1 Introduction

Deep inelastic scattering (DIS) of leptons off nucleons has proved to be a key process in the understanding of the structure of the proton and testing of the Standard Model (SM). Neutral current (NC) DIS is mediated by photons and Z bosons and is sensitive to all quark flavours. However, at leading order only up-type quarks and down-type antiquarks contribute to $e^- p$ charged current (CC) DIS. Thus this process is a powerful probe of flavour-specific parton distribution functions (PDFs). Due to the chiral nature of the weak interaction, the SM predicts a linear dependence of the CC cross section on the degree of longitudinal polarisation of the electron beam. The cross section is expected to be zero for a right-handed electron beam.

The HERA ep collider allowed the exploration of CC DIS [1–12] up to much higher Q^2 than previously possible in fixed-target experiments [13–16]. This paper presents measurements of the cross sections for $e^- p$ CC DIS with longitudinally polarised electron beams. The measured cross sections are compared to SM predictions and previous ZEUS measurements of $e^+ p$ CC DIS with longitudinally polarised positron beams [17]. Similar results in $e^+ p$ CC DIS have been published by the H1 Collaboration [18].

2 Kinematic variables and cross sections

Deep inelastic lepton-proton scattering can be described in terms of the kinematic variables x, y and Q^2. The variable Q^2 is defined as $Q^2 = -q^2 = -(k - k')^2$ where k and k' are the four-momenta of the incoming and scattered lepton, respectively. Bjorken x is defined by $x = Q^2/2P \cdot q$ where P is the four-momentum of the incoming proton. The variable y is defined by $y = P \cdot q / P \cdot k$. The variables x, y and Q^2 are related by $Q^2 = sxy$, where $s = 4E_e E_p$ is the square of the lepton-proton centre-of-mass energy (neglecting the masses of the incoming particles) and E_e and E_p are the energies of the incoming electron and proton, respectively.

The longitudinal polarisation of the electron beam, P_e, is defined as

$$P_e = \frac{N_R - N_L}{N_R + N_L},$$

where N_R and N_L are the numbers of right- and left-handed electrons in the beam. The electroweak Born-level cross section for the CC reaction, $e^- p \to \nu_e X$, with longitudinally polarised electron beams, can be expressed as [19]

$$\frac{d^2\sigma^{\mathrm{CC}}(e^- p)}{dx dQ^2} = (1 - P_e)\frac{G_F^2}{4\pi x}\left(\frac{M_W^2}{M_W^2 + Q^2}\right)^2 \left[Y_+ F_2^{\mathrm{CC}}(x, Q^2) + Y_- x F_3^{\mathrm{CC}}(x, Q^2) - y^2 F_L(x, Q^2)\right],$$

where G_F is the Fermi constant, M_W is the mass of the W boson and $Y_\pm = 1 \pm (1-y)^2$. The longitudinal structure function gives a negligible contribution to the cross section, except at values of y close to 1. Within the framework of the quark-parton model, the structure functions $F_2^{\rm CC}$ and $xF_3^{\rm CC}$ for $e^- p$ collisions can be written in terms of sums and differences of quark and anti-quark PDFs as follows:

$$F_2^{\rm CC} = x[u(x,Q^2) + c(x,Q^2) + \bar{d}(x,Q^2) + \bar{s}(x,Q^2)],$$

$$xF_3^{\rm CC} = x[u(x,Q^2) + c(x,Q^2) - \bar{d}(x,Q^2) - \bar{s}(x,Q^2)],$$

where, for example, the PDF $u(x,Q^2)$ gives the number density of up quarks with momentum-fraction x at a given Q^2. Since the top-quark mass is large and the off-diagonal elements of the CKM matrix are small [20], the contribution from third-generation quarks may be ignored [21].

3 Experimental apparatus

A detailed description of the ZEUS detector can be found elsewhere [22]. A brief outline of the components most relevant for this analysis is given below.

Charged particles were tracked in the central tracking detector (CTD) [23], which operated in a magnetic field of 1.43 T provided by a thin superconducting solenoid. The CTD consisted of 72 cylindrical drift chamber layers, organised in nine superlayers covering the polar-angle[1] region $15^\circ < \theta < 164^\circ$. A silicon microvertex detector (MVD) [24] was installed between the beampipe and the inner radius of the CTD. The MVD was organised into a barrel with three cylindrical layers and a forward section with four planar layers perpendicular to the HERA beam direction. Charged-particle tracks were reconstructed using information from the CTD and MVD.

The high-resolution uranium–scintillator calorimeter (CAL) [25] consisted of three parts: the forward (FCAL), the barrel (BCAL) and the rear (RCAL) calorimeter, covering 99.7% of the solid angle around the nominal interaction point. Each part was subdivided transversely into towers and longitudinally into one electromagnetic section (EMC) and either one (in RCAL) or two (in BCAL and FCAL) hadronic sections (HAC). The smallest subdivision of the calorimeter was called a cell. The CAL relative energy resolutions, as measured under test-beam conditions, were $\sigma(E)/E = 0.18/\sqrt{E}$ for electrons and

[1] The ZEUS coordinate system is a right-handed Cartesian system, with the Z axis pointing in the proton beam direction, referred to as the "forward direction", and the X axis pointing left towards the centre of HERA. The polar angle, θ, is measured with respect to the proton beam direction. The coordinate origin is at the nominal interaction point.

$\sigma(E)/E = 0.35/\sqrt{E}$ for hadrons, with E in GeV. The timing resolution of the CAL was better than 1 ns for energy deposits exceeding 4.5 GeV.

An iron structure that surrounded the CAL was instrumented as a backing calorimeter (BAC) [26] to measure energy leakage from the CAL. Muon chambers in the forward, barrel and rear [27] regions were used in this analysis to veto background events induced by cosmic-ray or beam-halo muons.

The luminosity was measured using the Bethe-Heitler reaction $ep \to e\gamma p$ with the luminosity detector which consisted of two independent systems, a photon calorimeter and a magnetic specrometer.

The lepton beam in HERA became naturally transversely polarised through the Sokolov-Ternov effect [28, 29]. The characteristic build-up time for the HERA accelerator was approximately 40 minutes. Spin rotators on either side of the ZEUS detector changed the transverse polarisation of the beam into longitudinal polarisation and back again. The electron beam polarisation was measured using two independent polarimeters, the transverse polarimeter (TPOL) [30] and the longitudinal polarimeter (LPOL) [31]. Both devices exploited the spin-dependent cross section for Compton scattering of circularly polarised photons off electrons to measure the beam polarisation. The luminosity and polarisation measurements were made over times that were much shorter than the polarisation build-up time.

The measurements are based on data samples collected with the ZEUS detector from 2004 to 2006 when HERA collided protons of energy 920 GeV with electrons of energy 27.5 GeV, yielding collisions at a centre-of-mass energy of 318 GeV. The integrated luminosities of the data samples were $104\,\mathrm{pb}^{-1}$ and $71\,\mathrm{pb}^{-1}$ at mean luminosity weighted polarisations of -0.27 and $+0.30$, respectively. Figure 1 shows the luminosity collected as a function of the longitudinal polarisation of the electron beam.

4 Monte Carlo simulation

Monte Carlo (MC) simulations were used to determine the efficiency for selecting events and the accuracy of kinematic reconstruction, to estimate the background rates from ep processes other than CC DIS and to extract cross sections for the full kinematic region. A sufficient number of events was generated to ensure that the statistical uncertainties arising from the MC simulation were negligible compared to those of the data. The MC samples were normalised to the total integrated luminosity of the data.

Charged current DIS events, including electroweak radiative effects, were simulated using the HERACLES 4.6.3 [32] program with the DJANGOH 1.3 [33] interface to the MC

generators that provide the hadronisation. Initial-state radiation, vertex and propagator corrections and two-boson exchange are included in HERACLES. The parameters of the SM were set to the PDG [20] values. The events were generated using the CTEQ5D [34] PDFs. The colour-dipole model of ARIADNE 4.10 [35] was used to simulate $\mathcal{O}(\alpha_S)$ plus leading-logarithmic corrections to the result of the quark-parton model. This program uses the Lund string model of JETSET 7.4 [36] for the hadronisation. A set of NC DIS events generated with DJANGOH was used to estimate the NC contamination in the CC sample. Photoproduction background was estimated using events simulated with HERWIG 5.9 [37]. The background from W production was estimated using the EPVEC 1.0 [38] generator, and the background from production of charged-lepton pairs was generated with the GRAPE 1.1 [39] program.

The vertex distribution in data is a crucial input to the MC simulation for the correct evaluation of the event-selection efficiency. Therefore, the Z-vertex distribution used in the MC simulation was determined from a sample of NC DIS events in which the event-selection efficiency was independent of Z.

The ZEUS detector response was simulated with a program based on GEANT 3.21 [40]. The simulated events were subjected to the same trigger requirements as the data, and processed by the same reconstruction programs.

5 Reconstruction of kinematic variables

The principal signature of CC DIS at HERA is large missing transverse momentum, $P_{T,\mathrm{miss}}$, arising from the energetic final-state neutrino which escapes detection. $P_{T,\mathrm{miss}}$ is related to the total hadronic momentum, P_T, by $P^2_{T,\mathrm{miss}} = (-\overrightarrow{P}_T)^2$, where

$$(\overrightarrow{P}_T)^2 = \left(\sum_i E_i \sin\theta_i \cos\phi_i\right)^2 + \left(\sum_i E_i \sin\theta_i \sin\phi_i\right)^2 .$$

The sums run over all CAL energy deposits, E_i (uncorrected in the trigger, but corrected [41] for energy loss in inactive material and reconstruction deficiencies in the offline analysis), and θ_i and ϕ_i are the polar and azimuthal angles of the calorimeter deposits. The polar angle of the hadronic system, γ_h, is defined by

$$\cos\gamma_h = ((\overrightarrow{P}_T)^2 - \delta^2)/((\overrightarrow{P}_T)^2 + \delta^2),$$

where $\delta = \sum_i E_i(1-\cos\theta_i) = \sum_i (E - P_Z)_i$. In the naive quark-parton model, γ_h is the angle of the scattered quark. Finally, the total transverse energy, E_T, is given by $E_T = \sum_i E_i \sin\theta_i$.

The ratio of the parallel, V_P, and anti-parallel, V_{AP}, components of the hadronic transverse momentum can be used to distinguish CC DIS from photoproduction events. These variables are defined as

$$V_P = \sum_i \overrightarrow{P}_{T,i} \cdot \overrightarrow{n}_{P_T} \quad \text{for} \quad \overrightarrow{P}_{T,i} \cdot \overrightarrow{n}_{P_T} > 0,$$

$$V_{AP} = -\sum_i \overrightarrow{P}_{T,i} \cdot \overrightarrow{n}_{P_T} \quad \text{for} \quad \overrightarrow{P}_{T,i} \cdot \overrightarrow{n}_{P_T} < 0,$$

where the sums are performed over all calorimeter cells and $\overrightarrow{n}_{P_T} = \overrightarrow{P}_T/P_T$.

The kinematic variables were reconstructed using the Jacquet-Blondel method [42]. The estimators of y, Q^2 and x are: $y_{\rm JB} = \delta/(2E_e)$, $Q^2_{\rm JB} = P_T^2/(1-y_{\rm JB})$, and $x_{\rm JB} = Q^2_{\rm JB}/(sy_{\rm JB})$.

The resolution in Q^2 is about 20%. The resolution in x improves from about 20% at $x = 0.01$ to about 5% at $x = 0.5$. The resolution in y ranges from about 14% at $y = 0.05$ to about 8% at $y = 0.83$.

6 Event selection

Charged current DIS candidates were selected by requiring a large $P_{T,\rm miss}$. The main sources of background came from NC DIS and high-E_T photoproduction in which the finite energy resolution of the CAL or energy that escapes detection can lead to significant measured missing transverse momentum. Non-ep events such as beam-gas interactions, beam-halo muons or cosmic rays can also cause substantial imbalance in the measured transverse momentum and constitute additional sources of background. The selection criteria described below were imposed to separate CC events from all backgrounds.

6.1 Trigger selection

ZEUS had a three-level trigger system [22,43,44]. At the first level, only coarse calorimeter and tracking information was available. Events were selected using criteria based on the energy, transverse energy and missing transverse momentum measured in the calorimeter. Generally, events were triggered with low thresholds on these quantities if a coincidence with CTD tracks from the event vertex occurred, while higher thresholds were required for events with no CTD tracks.

At the second level, timing information from the calorimeter was used to reject events inconsistent with the bunch-crossing time. In addition, the topology of the CAL energy deposits was used to reject background events. In particular, a tighter cut was made

on missing transverse momentum, since the resolution in this variable was better at the second level than at the first level.

At the third level, full track reconstruction and vertex finding were performed and used to reject candidate events with a vertex inconsistent with an *ep* interaction. Cuts were applied to calorimeter quantities and reconstructed tracks to further reduce beam-gas contamination.

6.2 Offline selection

When γ_h is large, charged-particle tracks can be used to reconstruct the event vertex, strongly suppressing non-*ep* backgrounds. For CC events with small γ_h, the charged particles of the hadronic final state are often outside the acceptance of the tracking detectors. Such events populate the high-x region of the kinematic plane. The events were classified according to γ_0, the value of γ_h measured with respect to the nominal interaction point. For events with large γ_0 the kinematic quantities were recalculated using the Z-coordinate of the event vertex ($Z_{\rm vtx}$) determined from charged-particle tracks.

In events with $\gamma_0 > 0.4$ rad a reconstructed vertex was required. Additional requirements for event selection are given below.

- selection of CC events:
  - $|Z_{\rm vtx}| < 50$ cm;
  - $P_{T,\rm miss} > 12$ GeV;
- rejection of beam-gas events:
  - $P'_{T,\rm miss} > 10\,\rm GeV$ and $P''_{T,\rm miss} > 8\,\rm GeV$ where $P'_{T,\rm miss}$ is the missing transverse momentum calculated excluding the ring of FCAL towers closest to the beam pipe and $P''_{T,\rm miss}$ is the corresponding quantity calculated excluding the two rings of FCAL towers closest to the beam pipe. These requirements strongly suppress beam-gas events while maintaining high efficiency for CC events;
  - tracks associated with the event vertex with transverse momentum in excess of 0.2 GeV and a polar angle in the range 15° to 164° were defined as "good" tracks. In order to remove beam-gas background, at least one such track was required and a cut was also applied in two dimensions on the number of good tracks versus the total number of tracks. This cut was $N_{\rm GoodTrks} > 0.3\dot{(}N_{\rm Trks} - 20)$;
- rejection of photoproduction:
  - $V_{AP}/V_P < 0.4$ was required for events with $P_{T,\rm miss} < 30\,\rm GeV$. For events with $P_{T,\rm miss} < 20\,\rm GeV$ this cut was tightened to $V_{AP}/V_P < 0.23$. This selected events with a collimated energy flow, as expected from a single scattered quark;

  - for charged current events, there is a correlation between the direction of the $P_{T,\mathrm{miss}}$ vector calculated using tracks and that obtained using the CAL. The difference between these quantities was required to be less than 0.5 radians for $P_{T,\mathrm{miss}} < 45\,\mathrm{GeV}$. As less background is expected for high $P_{T,\mathrm{miss}}$ this requirement was loosened to less than 1.0 radian for $P_{T,\mathrm{miss}} \geq 45\,\mathrm{GeV}$;

- rejection of NC DIS: NC DIS events in which the energies of the scattered electron or the jet are poorly measured can have a considerable apparent missing transverse momentum. To identify such events, a search for candidate electrons was made using isolated electromagnetic clusters in the CAL [45] for events with $P_{T,\mathrm{miss}} < 30\,\mathrm{GeV}$. Candidate electron clusters within the tracking acceptance were required to have an energy above $4\,\mathrm{GeV}$ and a matching track. Clusters with $\theta > 164^\circ$ were required to have a transverse momentum exceeding $2\,\mathrm{GeV}$. Events with a candidate electron satisfying the above criteria and $\delta > 30\,\mathrm{GeV}$ were rejected, since for fully contained NC events, δ peaks at $2E_e = 55\,\mathrm{GeV}$;

- rejection of non-ep background: muon-finding algorithms based on CAL energy deposits or muon-chamber signals were used to reject events produced by cosmic rays or muons in the beam halo.

In events with $\gamma_0 < 0.4$ rad some requirements were tightened to compensate for the relaxation of the track requirements. Additional requirements for event selection are given below.

- missing transverse momentum: events were required to satisfy $P_{T,\mathrm{miss}} > 14\,\mathrm{GeV}$ and $P'_{T,\mathrm{miss}} > 12\,\mathrm{GeV}$;

- rejection of non-ep background: A class of background events arose from beam-halo muons that produced a shower inside the FCAL. To reduce this background, in addition to the muon-rejection cuts described above, topological cuts on the transverse and longitudinal shower shape were imposed. These cuts rejected events in which the energy deposits were more collimated than for typical hadronic jets.

The kinematic region was restricted to $Q^2_{\mathrm{JB}} > 200\,\mathrm{GeV}^2$ and $y_{\mathrm{JB}} < 0.9$ to ensure good resolution.

A total of 7198 events satisfied these criteria. A background contamination from ep processes of 0.5%, dominated by the photoproduction component, is predicted. Figure 2 compares the distributions of data events entering the final CC sample with the MC expectation for the sum of the CC signal and ep background events. The MC simulations give a reasonable description of the data.

7 Cross-section determination and systematic uncertainties

The measured cross section in a particular kinematic bin, for example for $d^2\sigma/dxdQ^2$, was determined from

$$\frac{d^2\sigma}{dxdQ^2} = \frac{N_{\rm data} - N_{\rm bg}}{N_{\rm MC}} \cdot \frac{d^2\sigma^{\rm SM}_{\rm Born}}{dxdQ^2},$$

where $N_{\rm data}$ is the number of data events, $N_{\rm bg}$ is the number of background events estimated from the MC simulation and $N_{\rm MC}$ is the number of signal MC events. The cross-section $\frac{d^2\sigma^{\rm SM}_{\rm Born}}{dxdQ^2}$ is the Standard Model prediction evaluated in the on-shell scheme [46] using the PDG values for the electroweak parameters and the CTEQ5D PDFs [34]. A similar procedure was used for $d\sigma/dQ^2$, $d\sigma/dx$ and $d\sigma/dy$. Consequently, the acceptance, as well as the bin-centring and radiative corrections were all taken from the MC simulation. The cross-sections $d\sigma/dQ^2$ and $d\sigma/dx$ were extrapolated to the full y range using the SM predictions calculated with the CTEQ5D PDFs.

The systematic uncertainties in the measured cross sections were determined by changing the analysis procedure in turn and repeating the extraction of the cross sections.

- calorimeter energy scale: the relative uncertainty of the hadronic energy scale was 2%. Varying the energy scale of the calorimeter by this amount in the detector simulation induces small shifts of the Jacquet-Blondel estimators of the kinematic variables. The variation of the energy scale for each of the calorimeters simultaneously up or down by this amount gave the systematic uncertainty on the total measured energy in the calorimeter. The resulting systematic shifts in the measured cross sections were typically within $\pm 5\%$, but increased to $\pm(20-30)\%$ in the highest Q^2 and x bins of the single-differential cross sections and reached $\pm 45\%$ in the double-differential cross section;
- reconstruction: an alternative analysis [47] was performed using jets to reconstruct the kinematic quantities and reject background. The difference between the nominal and jet analyses was taken as an estimate of the systematic uncertainity on the reconstruction and background rejection. The difference was found to be typically within $\pm 10\%$, but increased up to $\pm(20-25)\%$ in the highest Q^2 and x bins of the cross sections;
- background subtraction: the uncertainty in the small contribution from photoproduction was estimated by varying the normalisation by $\pm 60\%$, resulting [48, 49] in modifications of the cross sections within $\pm 2\%$;

- selection criteria: in order to estimate the bias introduced into the measurements from an imperfect description of the data by the MC simulation, the efficiencies for each of the selection criteria were measured using the hadronic final state in NC DIS data. Using the measured efficiencies to extract the cross sections instead of the CC MC gave changes in the cross sections that were typically within $\pm 2\%$, except for the two-dimensional tracking cut which gave an effect of 10% at high Q^2;
- the uncertainties associated with the trigger, choice of PDFs in the MC and the measurement of the vertex positions were negligible.

The individual uncertainties were added in quadrature separately for the positive and negative deviations from the nominal cross-section values to obtain the total systematic uncertainties. The $\mathcal{O}(\alpha)$ electroweak corrections to CC DIS have been discussed by several authors [50, 51]. Various theoretical approximations and computer codes gave differences in the CC cross sections of typically $\pm(1-2)\%$ or less. However, the differences can be as large as $\pm(3-8)\%$ at high x and high y. No uncertainty was included in the measured cross sections from this source.

The relative uncertainty in the measured polarisation was 3.6% using the LPOL and 4.2% using the TPOL. The choice of polarimeter measurement was made on a run-by-run basis. The LPOL measurement was used when available, otherwise the TPOL measurement was used. The uncertainty of 2.6% on the measured total luminosity was not included in the differential cross-section figures or the tables.

8 Results

The total cross section, corrected to the Born level of the electroweak interaction, for $e^- p$ CC DIS in the kinematic region $Q^2 > 200\,\mathrm{GeV}^2$ was measured to be

$$\sigma^{\mathrm{CC}}(P_e = +0.30 \pm 0.01) = 47.1 \pm 1.1(\mathrm{stat.}) \pm 2.2(\mathrm{syst.})\ \mathrm{pb},$$

$$\sigma^{\mathrm{CC}}(P_e = -0.27 \pm 0.01) = 83.1 \pm 1.2(\mathrm{stat.}) \pm 3.3(\mathrm{syst.})\ \mathrm{pb}.$$

The uncertainty in the measured luminosity is included in the systematic uncertainty. The total cross section is shown as a function of the longitudinal polarisation of the lepton beam in Fig. 3, including previous ZEUS measurements from both $e^- p$ and $e^+ p$ data [11, 12, 17]. Figure 4 shows only the $e^- p$ data, with a finer binning to emphasise the dependence on the lepton beam polarisation. The cross-section values are tabulated in Table 1. The data are compared to the SM predictions evaluated at next-to-leading-order in QCD using the ZEUS-JETS [52], CTEQ6D [53] and MRST04 [54] PDFs which describe the data well.

The single-differential cross-sections $d\sigma/dQ^2$, $d\sigma/dx$ and $d\sigma/dy$ for CC DIS are shown in Figs. 5, 6 and 7 and given in Tables 2, 3 and 4. A clear difference is observed between the measurements for positive and negative longitudinal polarisation, which is independent of the kinematic variables. The effects are well described by the SM evaluated using the ZEUS-JETS, CTEQ6D and MRST04 PDFs. The precision of the data is comparable to the uncertainties in the SM predictions, therefore these data have the potential to further constrain the PDFs.

The reduced double-differential cross section, $\tilde{\sigma}$, is defined as

$$\tilde{\sigma} = \left[\frac{G_F^2}{2\pi x} \left(\frac{M_W^2}{M_W^2 + Q^2} \right)^2 \right]^{-1} \frac{d^2\sigma}{dx\, dQ^2}.$$

At leading order in QCD, $\tilde{\sigma}(e^- p \to \nu_e X)$ depends on the quark momentum distributions as follows:

$$\tilde{\sigma}(e^- p \to \nu_e X) = x \left[u + c + (1-y)^2 (\bar{d} + \bar{s}) \right].$$

The reduced cross section was measured in the kinematic range $280 < Q^2 < 30\,000\,\mathrm{GeV}^2$ and $0.015 < x < 0.65$ and is shown as a function of x, at fixed values of Q^2 in Fig. 8 and tabulated in Tables 5, 6 and 7. The data points were corrected to $P_e = 0$ using the SM prediction. The predictions of the SM evaluated using the ZEUS-JETS, CTEQ6D and MRST04 PDFs give a good description of the data. The contributions from the PDF combinations $(u + c)$ and $(\bar{d} + \bar{s})$, obtained in the $\overline{\mathrm{MS}}$ scheme from the ZEUS-JETS fit, are shown separately.

The W boson couples only to left-handed fermions and right-handed anti-fermions. Therefore, the angular distribution of the scattered quark in $e^- q$ CC DIS will be flat in the electron-quark centre-of-mass scattering angle, θ^*, while it will exhibit a $(1 + \cos\theta^*)^2$ distribution in $e^- \bar{q}$ scattering. Since $(1-y)^2 \propto (1 + \cos\theta^*)^2$, the helicity structure of CC interactions can be illustrated by plotting the reduced double-differential cross section versus $(1-y)^2$ in bins of x. This is shown in Fig. 9. In the region of approximate scaling, i.e. $x \sim 0.1$, this yields a straight line. At leading order in QCD, the intercept of this line gives the $(u + c)$ contribution, while the slope gives the $(\bar{d} + \bar{s})$ contribution.

9 Summary

The cross sections for charged current deep inelastic scattering in $e^- p$ collisions with longitudinally polarised electron beams have been measured. The measurements are based on a data sample with an integrated luminosity of $175\,\mathrm{pb}^{-1}$ collected with the ZEUS detector at HERA at a centre-of-mass energy of 318 GeV. The total cross section is given

for positive and negative values of the longitudinal polarisation of the electron beam. In addition, the differential cross-sections $d\sigma/dQ^2$, $d\sigma/dx$ and $d\sigma/dy$ for $Q^2 > 200\,\mathrm{GeV}^2$ and $d^2\sigma/dxdQ^2$ are presented in the kinematic range $280 < Q^2 < 30\,000\,\mathrm{GeV}^2$ and $0.015 < x < 0.65$. Overall the measured cross sections are well described by the predictions of the Standard Model.

Acknowledgements

We appreciate the contributions to the construction and maintenance of the ZEUS detector of many people who are not listed as authors. The HERA machine group and the DESY computing staff are especially acknowledged for their success in providing excellent operation of the collider and the data-analysis environment. We thank the DESY directorate for their strong support and encouragement. It is also a pleasure to thank H. Spiesberger and W. Hollik for helpful discussions.

References

[1] H1 Collab., T. Ahmed et al., Phys. Lett. **B 324**, 241 (1994).

[2] H1 Collab., S. Aid et al., Z. Phys. **C 67**, 565 (1995).

[3] H1 Collab., S. Aid et al., Phys. Lett. **B 379**, 319 (1996).

[4] H1 Collab., C. Adloff et al., Eur. Phys. J. **C 13**, 609 (2000).

[5] H1 Collab., C. Adloff et al., Eur. Phys. J. **C 19**, 269 (2001).

[6] H1 Collab., C. Adloff et al., Eur. Phys. J. **C 21**, 33 (2001).

[7] H1 Collab., C. Adloff et al., Eur. Phys. J. **C 30**, 1 (2003).

[8] ZEUS Collab., M. Derrick et al., Phys. Rev. Lett. **75**, 1006 (1995).

[9] ZEUS Collab., M. Derrick et al., Z. Phys. **C 72**, 47 (1996).

[10] ZEUS Collab., J. Breitweg et al., Eur. Phys. J. **C 12**, 411 (2000). Erratum in Eur. Phys. J. **C 27**, 305 (2003).

[11] ZEUS Collab., S. Chekanov et al., Phys. Lett. **B 539**, 197 (2002). Erratum in Phys. Lett. **B 552**, 308 (2003).

[12] ZEUS Collab., S. Chekanov et al., Eur. Phys. J. **C 32**, 1 (2003).

[13] CDHS Collab., H. Abramowicz et al., Z. Phys. **C 25**, 29 (1984).

[14] CDHSW Collab., J.P. Berge et al., Z. Phys. **C 49**, 187 (1991).

[15] CCFR Collab., E. Oltman et al., Z. Phys. **C 53**, 51 (1992).

[16] BEBC Collab., G.T. Jones et al., Z. Phys. **C 62**, 575 (1994).

[17] ZEUS Collab., S. Chekanov et al., Phys. Lett. **B 637**, 210 (2006).

[18] H1 Collab., A. Aktas et al., Phys. Lett. **B 634**, 173 (2006).

[19] R. Devenish and A.M. Cooper-Sarkar, *Deep Inelastic Scattering*. Oxford University Press, 2003.

[20] Particle Data Group, W.-M. Yao et al., J. Phys. **G 33**, 1 (2006).

[21] U.F. Katz, *Deep-Inelastic Positron–Proton Scattering in the High-Momentum-Transfer Regime of HERA*, Springer Tracts in Modern Physics, Vol. 168. Springer, Berlin, Heidelberg, 2000.

[22] ZEUS Collab., U. Holm (ed.), *The ZEUS Detector*. Status Report (unpublished), DESY (1993), available on `http://www-zeus.desy.de/bluebook/bluebook.html`.

[23] N. Harnew et al., Nucl. Instr. and Meth. **A 279**, 290 (1989);
B. Foster et al., Nucl. Phys. Proc. Suppl. **B 32**, 181 (1993);
B. Foster et al., Nucl. Instr. and Meth. **A 338**, 254 (1994).

[24] A. Polini et al., Nucl. Instr. and Meth. **A 581**, 656 (2007).

[25] M. Derrick et al., Nucl. Instr. and Meth. **A 309**, 77 (1991);
A. Andresen et al., Nucl. Instr. and Meth. **A 309**, 101 (1991);
A. Caldwell et al., Nucl. Instr. and Meth. **A 321**, 356 (1992);
A. Bernstein et al., Nucl. Instr. and Meth. **A 336**, 23 (1993).

[26] H. Abramowicz et al., Nucl. Instr. and Meth. **A 313**, 126 (1992).

[27] G. Abbiendi et al., Nucl. Instr. and Meth. **A 333**, 342 (1993).

[28] A.A. Sokolov and I.M. Ternov, Sov. Phys. Dokl. **8**, 1203 (1964).

[29] V. N. Baier and V. A. Khoze, Sov. J. Nucl. Phys. **B 9**, 238 (1969).

[30] D.P. Barber et al., Nucl. Instr. and Meth. **A 329**, 79 (1993).

[31] M. Beckmann et al., Nucl. Instr. and Meth. **A 479**, 334 (2002).

[32] A. Kwiatkowski, H. Spiesberger and H.-J. Möhring, Comp. Phys. Comm. **69**, 155 (1992). Also in *Proc. Workshop Physics at HERA*, eds. W. Buchmüller and G.Ingelman, (DESY, Hamburg, 1991);
H. Spiesberger, *An Event Generator for ep Interactions at HERA Including Radiative Processes (Version 4.6)*, 1996, available on `http://www.desy.de/~hspiesb/heracles.html`.

[33] H. Spiesberger, HERACLES *and* DJANGOH*: Event Generation for ep Interactions at HERA Including Radiative Processes*, 1998, available on `http://www.desy.de/~hspiesb/djangoh.html`.

[34] CTEQ Collab., H.L. Lai et al., Eur. Phys. J. **C 12**, 375 (2000).

[35] L. Lönnblad, Comp. Phys. Comm. **71**, 15 (1992).

[36] T. Sjöstrand, Comp. Phys. Comm. **39**, 347 (1986);
T. Sjöstrand and M. Bengtsson, Comp. Phys. Comm. **43**, 367 (1987);
T. Sjöstrand, Comp. Phys. Comm. **82**, 74 (1994).

[37] G. Marchesini et al., Comp. Phys. Comm. **67**, 465 (1992).

[38] U. Baur, J.A.M. Vermaseren and D. Zeppenfeld, Nucl. Phys. **B 375**, 3 (1992).

[39] T. Abe, Comp. Phys. Comm. **136**, 126 (2001).

[40] R. Brun et al., GEANT3, Technical Report CERN-DD/EE/84-1, CERN, 1987.

[41] ZEUS Collab., J. Breitweg et al., Eur. Phys. J. **C 11**, 427 (1999).

[42] F. Jacquet and A. Blondel, *Proceedings of the Study for an ep Facility for Europe*, U. Amaldi (ed.), p. 391. Hamburg, Germany (1979). Also in preprint DESY 79/48.

[43] W.H. Smith, K. Tokushuku and L.W. Wiggers, *Proc. Computing in High-Energy Physics (CHEP), Annecy, France, Sept. 1992*, C. Verkerk and W. Wojcik (eds.), p. 222. CERN, Geneva, Switzerland (1992). Also in preprint DESY 92-150B.

[44] P. Allfrey et al., Nucl. Instr. and Meth. **A 580**, 1257 (2007).

[45] H. Abramowicz, A. Caldwell and R. Sinkus, Nucl. Instr. and Meth. **A 365**, 508 (1995);
R. Sinkus and T. Voss, Nucl. Instr. and Meth. **A 391**, 360 (1997).

[46] Particle Data Group, D.E. Groom et al., Eur. Phys. J. **C 15**, 1 (2000).

[47] J. Šutiak. Ph.D. Thesis, Max-Planck-Institute für Physik, München, 2006. (unpublished).

[48] C. Fry. Ph.D. Thesis, Imperial College London, 2007. (unpublished).

[49] H. Kaji. Ph.D. Thesis, Tokyo Metropolitan University, 2006. (unpublished).

[50] A.M. Cooper-Sarkar et al., J. Phys. **G 25**, 1387 (1999).

[51] B. Heinemann, S. Riess and H. Spiesberger, *Proc. Workshop on Monte Carlo Generators for HERA Physics*, G. Grindhammer et al. (ed.), p. 530. DESY, Hamburg, Germany (1999). Also in preprint DESY-PROC-1999-02, available on `http://www.desy.de/~heramc/`.

[52] ZEUS Collab., S. Chekanov et al., Eur. Phys. J. **C 42**, 1 (2005).

[53] J. Pumplin et al., JHEP **07** (2002).

[54] A.D. Martin et al., Phys. Lett. **B 604**, 61 (2004).

P_e	σ^{CC} (pb)
-0.32 ± 0.01	$89.7 \pm 2.9 \pm 3.6$
-0.29 ± 0.01	$81.9 \pm 2.9 \pm 3.3$
-0.27 ± 0.01	$82.0 \pm 2.9 \pm 3.3$
-0.23 ± 0.01	$78.2 \pm 2.5 \pm 3.1$
-0.16 ± 0.01	$72.5 \pm 2.6 \pm 2.9$
$+0.15 \pm 0.01$	$58.7 \pm 2.6 \pm 2.7$
$+0.25 \pm 0.01$	$48.4 \pm 2.3 \pm 2.3$
$+0.32 \pm 0.01$	$47.1 \pm 2.3 \pm 2.2$
$+0.36 \pm 0.01$	$38.7 \pm 2.3 \pm 1.8$

Table 1: *Values of the total cross section with statistical and systematic uncertainties.*

Q^2 range (GeV^2)	Q^2 (GeV^2)	$d\sigma/dQ^2$ (pb/ GeV^2)	
		$P_e = +0.30$	$P_e = -0.27$
$200 - 400$	280	$(3.00 \pm 0.25 \pm 0.21) \cdot 10^{-2}$	$(5.13 \pm 0.27\ ^{+0.37}_{-0.36}) \cdot 10^{-2}$
$400 - 711$	530	$(1.93 \pm 0.13 \pm 0.08) \cdot 10^{-2}$	$(3.57 \pm 0.15 \pm 0.15) \cdot 10^{-2}$
$711 - 1265$	950	$(1.40 \pm 0.08 \pm 0.05) \cdot 10^{-2}$	$(2.30 \pm 0.08 \pm 0.09) \cdot 10^{-2}$
$1265 - 2249$	1700	$(8.86 \pm 0.44\ ^{+0.31}_{-0.29}) \cdot 10^{-3}$	$(1.49 \pm 0.05\ ^{+0.05}_{-0.04}) \cdot 10^{-2}$
$2249 - 4000$	3000	$(4.19 \pm 0.22 \pm 0.27) \cdot 10^{-3}$	$(8.14 \pm 0.26 \pm 0.24) \cdot 10^{-3}$
$4000 - 7113$	5300	$(1.99 \pm 0.12\ ^{+0.10}_{-0.09}) \cdot 10^{-3}$	$(3.46 \pm 0.13 \pm 0.17) \cdot 10^{-3}$
$7113 - 12469$	9500	$(6.74 \pm 0.53\ ^{+0.61}_{-0.58}) \cdot 10^{-4}$	$(1.34 \pm 0.06 \pm 0.12) \cdot 10^{-3}$
$12469 - 22494$	17000	$(1.65 \pm 0.19\ ^{+0.25}_{-0.21}) \cdot 10^{-4}$	$(2.88 \pm 0.21\ ^{+0.43}_{-0.36}) \cdot 10^{-4}$
$22494 - 60000$	30000	$(3.47 \pm 0.67\ ^{+1.36}_{-1.20}) \cdot 10^{-5}$	$(5.50 \pm 0.71\ ^{+1.85}_{-1.54}) \cdot 10^{-5}$
x range	x	$d\sigma/dx$ (pb)	
		$P_e = +0.30$	$P_e = -0.27$
$0.01 - 0.021$	0.015	$424.6 \pm 33.4\ ^{+24.3}_{-23.4}$	$730.1 \pm 36.3\ ^{+50.6}_{-49.3}$
$0.021 - 0.046$	0.032	$302.2 \pm 16.2\ ^{+21.7}_{-21.4}$	$573.9 \pm 18.6\ ^{+36.1}_{-35.6}$
$0.046 - 0.1$	0.068	$210.5 \pm 9.2\ ^{+7.7}_{-7.6}$	$352.1 \pm 9.9\ ^{+12.5}_{-12.3}$
$0.1 - 0.178$	0.13	$119.5 \pm 5.9\ ^{+4.4}_{-4.4}$	$202.9 \pm 6.4 \pm 7.8$
$0.237 - 0.316$	0.24	$53.0 \pm 3.0\ ^{+2.8}_{-2.7}$	$104.4 \pm 3.5\ ^{+5.1}_{-4.9}$
$0.316 - 0.562$	0.42	$18.8 \pm 1.5\ ^{+1.9}_{-1.7}$	$32.0 \pm 1.6\ ^{+3.1}_{-2.8}$
$0.562 - 1$	0.65	$1.69^{+0.78\ +0.49}_{-0.56\ -0.42}$	$5.33 \pm 0.84\ ^{+1.75}_{-1.56}$
y range	y	$d\sigma/dy$ (pb)	
		$P_e = +0.30$	$P_e = -0.27$
$0.0 - 0.1$	0.05	$118.6 \pm 6.4 \pm 5.4$	$210.2 \pm 7.1\ ^{+10.3}_{-10.2}$
$0.1 - 0.2$	0.15	$80.2 \pm 3.9 \pm 2.3$	$137.9 \pm 4.3 \pm 2.7$
$0.2 - 0.34$	0.27	$57.0 \pm 2.8 \pm 2.1$	$101.5 \pm 3.1 \pm 3.7$
$0.34 - 0.48$	0.41	$41.9 \pm 2.5 \pm 1.9$	$73.7 \pm 2.7 \pm 3.8$
$0.48 - 0.62$	0.55	$36.4 \pm 2.4 \pm 2.2$	$62.5 \pm 2.6 \pm 4.2$
$0.62 - 0.76$	0.69	$27.3 \pm 2.2\ ^{+1.4}_{-1.3}$	$55.6 \pm 2.6\ ^{+2.8}_{-2.7}$
$0.76 - 0.9$	0.83	$24.5 \pm 2.4\ ^{+2.2}_{-2.1}$	$44.6 \pm 2.6\ ^{+4.9}_{-4.7}$

Table 2: *Values of the differential cross-sections $d\sigma/dQ^2$, $d\sigma/dx$ and $d\sigma/dy$ for $P_e = +0.30 \pm 0.01$ and $P_e = -0.27 \pm 0.01$. The following quantities are given: the range of the measurement; the value at which the cross section is quoted and the measured cross section, with statistical and systematic uncertainties.*

$d\sigma/dQ^2$					
Q^2 (GeV^2)	$d\sigma/dQ^2$ (pb/ GeV^2)	$\delta_{\rm stat}$ (%)	$\delta_{\rm syst}$ (%)	$\delta_{\rm unc}$ (%)	$\delta_{\rm es}$ (%)
280	$3.00 \cdot 10^{-2}$	± 8.5	$^{+7.1}_{-6.9}$	$^{+5.4}_{-5.4}$	$^{+4.6}_{-4.2}$
530	$1.93 \cdot 10^{-2}$	± 7.0	$^{+4.2}_{-4.2}$	$^{+2.0}_{-2.0}$	$^{+3.7}_{-3.7}$
950	$1.40 \cdot 10^{-2}$	± 5.6	$^{+3.4}_{-3.5}$	$^{+2.1}_{-2.1}$	$^{+2.6}_{-2.8}$
1700	$8.86 \cdot 10^{-3}$	± 5.0	$^{+3.5}_{-3.3}$	$^{+3.0}_{-3.0}$	$^{+1.7}_{-1.3}$
3000	$4.19 \cdot 10^{-3}$	± 5.4	$^{+6.4}_{-6.4}$	$^{+6.4}_{-6.4}$	$^{-0.1}_{+0.2}$
5300	$1.99 \cdot 10^{-3}$	± 5.9	$^{+4.8}_{-4.7}$	$^{+4.2}_{-4.2}$	$^{-1.9}_{+2.3}$
9500	$6.74 \cdot 10^{-4}$	± 7.8	$^{+9.0}_{-8.5}$	$^{+7.0}_{-7.0}$	$^{-4.9}_{+5.7}$
17000	$1.65 \cdot 10^{-4}$	± 11.8	$^{+15.2}_{-12.6}$	$^{+8.1}_{-8.1}$	$^{-9.7}_{+12.9}$
30000	$3.47 \cdot 10^{-5}$	± 19.4	$^{+39.3}_{-34.5}$	$^{+27.6}_{-27.6}$	$^{-20.6}_{+27.9}$
$d\sigma/dx$					
x	$d\sigma/dx$ (pb)	$\delta_{\rm stat}$ (%)	$\delta_{\rm syst}$ (%)	$\delta_{\rm unc}$ (%)	$\delta_{\rm es}$ (%)
0.015	424.6	± 7.9	$^{+5.7}_{-5.5}$	$^{+3.9}_{-3.9}$	$^{+4.2}_{-3.9}$
0.032	302.2	± 5.4	$^{+7.2}_{-7.1}$	$^{+6.6}_{-6.6}$	$^{+2.7}_{-2.5}$
0.068	210.5	± 4.4	$^{+3.6}_{-3.6}$	$^{+3.5}_{-3.5}$	$^{+1.2}_{-1.0}$
0.13	119.5	± 4.9	$^{+3.7}_{-3.7}$	$^{+3.6}_{-3.6}$	$^{-0.2}_{+0.4}$
0.24	53.0	± 5.6	$^{+5.2}_{-5.1}$	$^{+4.2}_{-4.2}$	$^{-2.8}_{+3.1}$
0.42	18.8	± 7.9	$^{+9.9}_{-8.9}$	$^{+5.2}_{-5.2}$	$^{-7.3}_{+8.5}$
0.65	1.69	$^{+46.1}_{-33.0}$	$^{+29.2}_{-25.0}$	$^{+13.9}_{-13.9}$	$^{-20.8}_{+25.7}$
$d\sigma/dy$					
y	$d\sigma/dy$ (pb)	$\delta_{\rm stat}$ (%)	$\delta_{\rm syst}$ (%)	$\delta_{\rm unc}$ (%)	$\delta_{\rm es}$ (%)
0.05	118.6	± 5.4	$^{+4.6}_{-4.5}$	$^{+4.3}_{-4.3}$	$^{+1.5}_{-1.4}$
0.15	80.2	± 4.9	$^{+2.9}_{-2.9}$	$^{+2.8}_{-2.8}$	$^{+0.6}_{-0.7}$
0.27	57.0	± 4.9	$^{+3.7}_{-3.7}$	$^{+3.6}_{-3.6}$	$^{+0.4}_{-0.4}$
0.41	41.9	± 5.9	$^{+4.6}_{-4.6}$	$^{+4.6}_{-4.6}$	$^{+0.3}_{+0.0}$
0.55	36.4	± 6.5	$^{+6.0}_{-6.1}$	$^{+6.0}_{-6.0}$	$^{-0.8}_{+0.4}$
0.69	27.3	± 7.9	$^{+5.0}_{-4.7}$	$^{+4.5}_{-4.5}$	$^{-1.3}_{+2.0}$
0.83	24.5	± 9.6	$^{+9.0}_{-8.4}$	$^{+6.5}_{-6.5}$	$^{-5.3}_{+6.2}$

Table 3: *Values of the differential cross-sections $d\sigma/dQ^2$, $d\sigma/dx$ and $d\sigma/dy$ for $P_e = +0.30 \pm 0.01$. The following quantities are given: the value at which the cross section is quoted; the measured cross section; the statistical uncertainty; the total systematic uncertainty; the uncorrelated systematic uncertainty and the calorimeter energy-scale uncertainty (δ_{es}), which has significant correlations between cross-section bins.*

$d\sigma/dQ^2$					
Q^2 (GeV^2)	$d\sigma/dQ^2$ (pb/ GeV^2)	δ_{stat} (%)	δ_{syst} (%)	δ_{unc} (%)	δ_{es} (%)
280	$5.13 \cdot 10^{-2}$	± 5.4	$^{+7.2}_{-6.9}$	$^{+5.5}_{-5.5}$	$^{+4.6}_{-4.2}$
530	$3.57 \cdot 10^{-2}$	± 4.3	$^{+4.1}_{-4.2}$	$^{+1.9}_{-1.9}$	$^{+3.7}_{-3.7}$
950	$2.30 \cdot 10^{-2}$	± 3.6	$^{+4.0}_{-4.0}$	$^{+2.9}_{-2.9}$	$^{+2.6}_{-2.8}$
1700	$1.49 \cdot 10^{-2}$	± 3.2	$^{+3.2}_{-3.0}$	$^{+2.6}_{-2.6}$	$^{+1.7}_{-1.3}$
3000	$8.14 \cdot 10^{-3}$	± 3.2	$^{+3.0}_{-3.0}$	$^{+3.0}_{-3.0}$	$^{-0.1}_{+0.2}$
5300	$3.46 \cdot 10^{-3}$	± 3.7	$^{+5.0}_{-4.8}$	$^{+4.4}_{-4.4}$	$^{-1.9}_{+2.3}$
9500	$1.34 \cdot 10^{-3}$	± 4.6	$^{+9.2}_{-8.7}$	$^{+7.2}_{-7.2}$	$^{-4.9}_{+5.7}$
17000	$2.88 \cdot 10^{-4}$	± 7.4	$^{+15.1}_{-12.5}$	$^{+7.8}_{-7.8}$	$^{-9.7}_{+12.9}$
30000	$5.50 \cdot 10^{-5}$	± 12.8	$^{+33.6}_{-27.9}$	$^{+18.8}_{-18.8}$	$^{-20.6}_{+27.9}$
$d\sigma/dx$					
x	$d\sigma/dx$ (pb)	δ_{stat} (%)	δ_{syst} (%)	δ_{unc} (%)	δ_{es} (%)
0.015	730.1	± 5.0	$^{+6.9}_{-6.7}$	$^{+5.5}_{-5.5}$	$^{+4.2}_{-3.9}$
0.032	573.9	± 3.2	$^{+6.3}_{-6.2}$	$^{+5.7}_{-5.7}$	$^{+2.7}_{-2.5}$
0.068	352.1	± 2.8	$^{+3.6}_{-3.5}$	$^{+3.4}_{-3.4}$	$^{+1.2}_{-1.0}$
0.13	202.9	± 3.1	$^{+3.9}_{-3.8}$	$^{+3.8}_{-3.8}$	$^{-0.2}_{+0.4}$
0.24	104.4	± 3.3	$^{+4.9}_{-4.7}$	$^{+3.8}_{-3.8}$	$^{-2.8}_{+3.1}$
0.42	32.0	± 5.0	$^{+9.8}_{-8.8}$	$^{+4.9}_{-4.9}$	$^{-7.3}_{+8.5}$
0.65	5.33	± 15.8	$^{+32.9}_{-29.2}$	$^{+20.6}_{-20.6}$	$^{-20.8}_{+25.7}$
$d\sigma/dy$					
y	$d\sigma/dy$ (pb)	δ_{stat} (%)	δ_{syst} (%)	δ_{unc} (%)	δ_{es} (%)
0.05	210.2	± 3.4	$^{+4.9}_{-4.9}$	$^{+4.6}_{-4.6}$	$^{+1.5}_{-1.4}$
0.15	137.9	± 3.1	$^{+1.9}_{-1.9}$	$^{+1.8}_{-1.8}$	$^{+0.6}_{-0.7}$
0.27	101.5	± 3.1	$^{+3.6}_{-3.6}$	$^{+3.6}_{-3.6}$	$^{+0.4}_{-0.4}$
0.41	73.7	± 3.7	$^{+5.2}_{-5.2}$	$^{+5.2}_{-5.2}$	$^{+0.3}_{+0.0}$
0.55	62.5	± 4.1	$^{+6.7}_{-6.8}$	$^{+6.7}_{-6.7}$	$^{-0.8}_{+0.4}$
0.69	55.6	± 4.6	$^{+5.1}_{-4.9}$	$^{+4.7}_{-4.7}$	$^{-1.3}_{+2.0}$
0.83	44.6	± 5.9	$^{+11.0}_{-10.6}$	$^{+9.1}_{-9.1}$	$^{-5.3}_{+6.2}$

Table 4: *Values of the differential cross-sections $d\sigma/dQ^2$, $d\sigma/dx$ and $d\sigma/dy$ for $P_e = -0.27 \pm 0.01$. The following quantities are given: the value at which the cross section is quoted; the measured cross section; the statistical uncertainty; the total systematic uncertainty; the uncorrelated systematic uncertainty and the calorimeter energy-scale uncertainty (δ_{es}), which has significant correlations between cross-section bins.*

Q^2 (GeV^2)	x	$\tilde{\sigma}$		
		$P_e = -0.27$	$P_e = +0.30$	$P_e = 0$
280	0.015	$1.39 \pm 0.14 \pm 0.11$	$1.03 \pm 0.15 \pm 0.07$	$1.17 \pm 0.10 \pm 0.08$
280	0.032	$1.54 \pm 0.14\ ^{+0.12}_{-0.11}$	$0.65 \pm 0.11 \pm 0.05$	$1.11 \pm 0.09\ ^{+0.09}_{-0.08}$
280	0.068	$1.54 \pm 0.17\ ^{+0.10}_{-0.11}$	$0.91 \pm 0.16\ ^{+0.05}_{-0.06}$	$1.21 \pm 0.12\ ^{+0.07}_{-0.08}$
280	0.13	$0.68^{+0.29\ +0.05}_{-0.21\ -0.03}$	$0.69^{+0.37\ +0.05}_{-0.26\ -0.03}$	$0.65 \pm 0.17\ ^{+0.04}_{-0.03}$
530	0.015	$1.46 \pm 0.12\ ^{+0.10}_{-0.09}$	$0.61 \pm 0.09 \pm 0.03$	$1.05 \pm 0.08 \pm 0.05$
530	0.032	$1.28 \pm 0.10 \pm 0.08$	$0.67 \pm 0.09 \pm 0.05$	$0.97 \pm 0.07 \pm 0.07$
530	0.068	$1.04 \pm 0.10 \pm 0.04$	$0.69 \pm 0.10\ ^{+0.03}_{-0.02}$	$0.84 \pm 0.07\ ^{+0.04}_{-0.03}$
530	0.13	$1.11 \pm 0.12\ ^{+0.04}_{-0.05}$	$0.69 \pm 0.12\ ^{+0.02}_{-0.03}$	$0.88 \pm 0.09\ ^{+0.03}_{-0.04}$
950	0.015	$1.14 \pm 0.10\ ^{+0.08}_{-0.09}$	$0.74 \pm 0.10 \pm 0.04$	$0.92 \pm 0.07 \pm 0.05$
950	0.032	$1.15 \pm 0.07 \pm 0.08$	$0.62 \pm 0.06 \pm 0.04$	$0.88 \pm 0.05 \pm 0.06$
950	0.068	$0.92 \pm 0.07 \pm 0.04$	$0.59 \pm 0.07 \pm 0.02$	$0.74 \pm 0.05 \pm 0.03$
950	0.13	$0.88 \pm 0.08 \pm 0.03$	$0.59 \pm 0.08\ ^{+0.01}_{-0.02}$	$0.72 \pm 0.05a \pm 0.02$
950	0.24	$0.68 \pm 0.08 \pm 0.02$	$0.40 \pm 0.08 \pm 0.01$	$0.53 \pm 0.06 \pm 0.02$
1700	0.032	$1.00 \pm 0.06 \pm 0.06$	$0.60 \pm 0.06 \pm 0.04$	$0.79 \pm 0.04 \pm 0.05$
1700	0.068	$0.94 \pm 0.05 \pm 0.04$	$0.60 \pm 0.05 \pm 0.03$	$0.76 \pm 0.04 \pm 0.03$
1700	0.13	$0.83 \pm 0.06 \pm 0.03$	$0.47 \pm 0.06\ ^{+0.02}_{-0.01}$	$0.64 \pm 0.04 \pm 0.02$
1700	0.24	$0.68 \pm 0.06 \pm 0.02$	$0.38 \pm 0.05 \pm 0.01$	$0.53 \pm 0.04 \pm 0.01$
1700	0.42	$0.41 \pm 0.07 \pm 0.02$	$0.19 \pm 0.05 \pm 0.01$	$0.30 \pm 0.05\ ^{+0.02}_{-0.01}$
3000	0.032	$0.96 \pm 0.08 \pm 0.07$	$0.44 \pm 0.07 \pm 0.04$	$0.70 \pm 0.06 \pm 0.06$
3000	0.068	$0.84 \pm 0.05 \pm 0.03$	$0.46 \pm 0.04 \pm 0.03$	$0.64 \pm 0.03 \pm 0.03$
3000	0.13	$0.72 \pm 0.05 \pm 0.03$	$0.45 \pm 0.05 \pm 0.03$	$0.58 \pm 0.04 \pm 0.03$
3000	0.24	$0.68 \pm 0.05 \pm 0.02$	$0.31 \pm 0.04 \pm 0.02$	$0.50 \pm 0.03 \pm 0.02$
3000	0.42	$0.33 \pm 0.04 \pm 0.02$	$0.12 \pm 0.03 \pm 0.01$	$0.23 \pm 0.02\ ^{+0.02}_{-0.01}$
5300	0.068	$0.80 \pm 0.05 \pm 0.04$	$0.45 \pm 0.05 \pm 0.02$	$0.62 \pm 0.04 \pm 0.03$
5300	0.13	$0.59 \pm 0.04 \pm 0.04$	$0.34 \pm 0.04 \pm 0.02$	$0.46 \pm 0.03 \pm 0.03$
5300	0.24	$0.55 \pm 0.04 \pm 0.03$	$0.29 \pm 0.04 \pm 0.02$	$0.42 \pm 0.03 \pm 0.02$
5300	0.42	$0.30 \pm 0.03 \pm 0.02$	$0.22 \pm 0.03 \pm 0.02$	$0.25 \pm 0.02 \pm 0.02$
5300	0.65	$0.11 \pm 0.03 \pm 0.03$		$0.07 \pm 0.02\ ^{+0.01}_{-0.02}$
9500	0.13	$0.81 \pm 0.06 \pm 0.07$	$0.37 \pm 0.05 \pm 0.03$	$0.59 \pm 0.04 \pm 0.05$
9500	0.24	$0.53 \pm 0.04\ ^{+0.06}_{-0.05}$	$0.27 \pm 0.04 \pm 0.03$	$0.40 \pm 0.03 \pm 0.04$
9500	0.42	$0.26 \pm 0.03\ ^{+0.03}_{-0.02}$	$0.14 \pm 0.03 \pm 0.01$	$0.20 \pm 0.02 \pm 0.02$
9500	0.65	$0.03^{+0.02}_{-0.01} \pm 0.01$	$0.03^{+0.03\ +0.01}_{-0.02\ -0.01}$	$0.03^{+0.02}_{-0.01} \pm 0.01$
17000	0.24	$0.52 \pm 0.05 \pm 0.07$	$0.25 \pm 0.04\ ^{+0.04}_{-0.03}$	$0.39 \pm 0.03 \pm 0.05$
17000	0.42	$0.20 \pm 0.03 \pm 0.03$	$0.14 \pm 0.03 \pm 0.02$	$0.17 \pm 0.02\ ^{+0.03}_{-0.02}$
17000	0.65	$0.05^{+0.03\ +0.02}_{-0.02\ -0.01}$		$0.03^{+0.02}_{-0.01} \pm 0.01$
30000	0.42	$0.26 \pm 0.04\ ^{+0.09}_{-0.07}$	$0.21 \pm 0.04\ ^{+0.08}_{-0.07}$	$0.23 \pm 0.03\ ^{+0.08}_{-0.07}$
30000	0.65	$0.05 \pm 0.02\ ^{+0.03}_{-0.02}$		$0.03^{+0.02\ +0.02}_{-0.01\ -0.01}$

Table 5: *Values of the reduced cross sections. The following quantities are given: the values of Q^2 and x at which the cross section is quoted and the measured cross section, with statistical and systematic uncertainties. Three bins in the $P_e = +0.30$ cross section were judged to be too statistically imprecise to be quoted without combination with the $P_e = -0.27$ data and are therefore omitted from the table.*

Q^2 (GeV^2)	x	$\tilde{\sigma}$	δ_{stat} (%)	δ_{syst} (%)	δ_{unc} (%)	δ_{es} (%)
280	0.015	1.03	± 14.7	$^{+7.2}_{-7.1}$	$^{+5.7}_{-5.7}$	$^{+4.3}_{-4.1}$
280	0.032	0.65	± 16.7	$^{+8.3}_{-7.7}$	$^{+7.3}_{-7.3}$	$^{+4.0}_{-2.4}$
280	0.068	0.91	± 17.2	$^{+5.9}_{-6.9}$	$^{+3.7}_{-3.7}$	$^{+4.6}_{-5.8}$
280	0.13	0.69	$^{+54.0}_{-37.1}$	$^{+6.5}_{-3.9}$	$^{+3.5}_{-3.5}$	$^{+5.5}_{-1.9}$
530	0.015	0.61	± 15.4	$^{+5.2}_{-4.8}$	$^{+2.9}_{-2.9}$	$^{+4.3}_{-3.8}$
530	0.032	0.67	± 12.6	$^{+7.4}_{-7.5}$	$^{+6.5}_{-6.5}$	$^{+3.4}_{-3.7}$
530	0.068	0.69	± 14.1	$^{+4.4}_{-3.6}$	$^{+2.1}_{-2.1}$	$^{+3.9}_{-2.9}$
530	0.13	0.69	± 16.8	$^{+3.1}_{-4.2}$	$^{+1.1}_{-1.1}$	$^{+2.9}_{-4.0}$
950	0.015	0.74	± 12.9	$^{+5.2}_{-5.9}$	$^{+4.2}_{-4.2}$	$^{+3.1}_{-4.2}$
950	0.032	0.62	± 10.4	$^{+7.2}_{-7.3}$	$^{+6.6}_{-6.6}$	$^{+2.9}_{-3.1}$
950	0.068	0.59	± 11.0	$^{+4.1}_{-4.0}$	$^{+3.0}_{-3.0}$	$^{+2.8}_{-2.7}$
950	0.13	0.59	± 12.9	$^{+2.0}_{-3.0}$	$^{+1.1}_{-1.1}$	$^{+1.7}_{-2.8}$
950	0.24	0.40	± 19.4	$^{+3.5}_{-2.9}$	$^{+2.3}_{-2.9}$	$^{+1.7}_{1.0}$
1700	0.032	0.60	± 9.3	$^{+7.1}_{-7.1}$	$^{+6.9}_{-6.9}$	$^{+1.8}_{-1.7}$
1700	0.068	0.60	± 8.7	$^{+4.4}_{-4.2}$	$^{+4.1}_{-4.1}$	$^{+1.7}_{-1.1}$
1700	0.13	0.47	± 12.2	$^{+3.8}_{-3.2}$	$^{+2.6}_{-2.6}$	$^{+2.8}_{-1.8}$
1700	0.24	0.38	± 12.9	$^{+3.4}_{-3.5}$	$^{+3.4}_{-3.3}$	$^{-0.3}_{-0.9}$
1700	0.42	0.19	± 29.0	$^{+5.7}_{-5.3}$	$^{+5.0}_{-5.0}$	$^{-2.0}_{+2.8}$
3000	0.032	0.44	± 15.6	$^{+9.7}_{-9.6}$	$^{+9.4}_{-9.4}$	$^{+2.5}_{-1.7}$
3000	0.068	0.46	± 8.8	$^{+7.0}_{-7.0}$	$^{+7.0}_{-7.0}$	$^{-0.0}_{-0.6}$
3000	0.13	0.45	± 10.6	$^{+7.2}_{-7.2}$	$^{+7.2}_{-7.2}$	$^{+0.2}_{+0.6}$
3000	0.24	0.31	± 12.2	$^{+6.4}_{-6.4}$	$^{+6.3}_{-6.3}$	$^{-0.9}_{+0.5}$
3000	0.42	0.12	± 21.4	$^{+8.9}_{-7.8}$	$^{+7.3}_{-7.3}$	$^{-2.8}_{+5.2}$
5300	0.068	0.45	± 10.6	$^{+5.0}_{-4.7}$	$^{+4.6}_{-4.6}$	$^{-1.0}_{+2.0}$
5300	0.13	0.34	± 11.0	$^{+6.1}_{-6.0}$	$^{+6.0}_{-6.0}$	$^{-0.8}_{+1.3}$
5300	0.24	0.29	± 12.6	$^{+5.3}_{-5.3}$	$^{+4.7}_{-4.7}$	$^{-2.6}_{+2.6}$
5300	0.42	0.22	± 13.9	$^{+7.2}_{-7.6}$	$^{+5.0}_{-5.0}$	$^{-5.7}_{+5.2}$
9500	0.13	0.37	± 12.2	$^{+8.3}_{-8.6}$	$^{+7.2}_{-7.2}$	$^{-4.6}_{+4.1}$
9500	0.24	0.27	± 13.4	$^{+11.1}_{-10.2}$	$^{+9.5}_{-9.5}$	$^{-3.9}_{+5.8}$
9500	0.42	0.14	± 18.3	$^{+10.4}_{-9.6}$	$^{+6.6}_{-6.6}$	$^{-7.0}_{+8.1}$
9500	0.650	0.03	$^{+97.4}_{-54.6}$	$^{+26.4}_{-21.3}$	$^{+14.5}_{-14.5}$	$^{-15.7}_{22.1}$
17000	0.24	0.25	± 15.9	$^{+14.2}_{-12.9}$	$^{+8.9}_{-8.9}$	$^{-9.3}_{+11.1}$
17000	0.42	0.14	± 21.4	$^{+16.8}_{-14.0}$	$^{+10.0}_{-10.0}$	$^{-9.8}_{+13.5}$
30000	0.42	0.21	± 20.9	$^{+38.3}_{-34.4}$	$^{+28.4}_{-28.4}$	$^{-19.5}_{+25.7}$

Table 6: *Values of the reduced cross section for $P_e = +0.30 \pm 0.01$. The following quantities are given: the values of Q^2 and x at which the cross section is quoted; the measured cross section; the statistical uncertainty; the total systematic uncertainty; the uncorrelated systematic uncertainty and the calorimeter energy-scale uncertainty (δ_{es}), which has significant correlations between cross-section bins.*

Q^2 (GeV^2)	x	$\tilde{\sigma}$	δ_{stat} (%)	δ_{syst} (%)	δ_{unc} (%)	δ_{es} (%)
280	0.015	1.39	± 10.4	$^{+8.2}_{-8.1}$	$^{+7.0}_{-7.0}$	$^{+4.3}_{-4.1}$
280	0.032	1.54	± 8.9	$^{+7.8}_{-7.1}$	$^{+6.7}_{-6.7}$	$^{+4.0}_{-2.4}$
280	0.068	1.54	± 11.0	$^{+6.3}_{-7.2}$	$^{+4.2}_{-4.2}$	$^{+4.6}_{-5.8}$
280	0.13	0.68	$^{+42.9}_{-31.3}$	$^{+7.0}_{-4.7}$	$^{+4.3}_{-4.3}$	$^{+5.5}_{-1.9}$
530	0.015	1.46	± 8.3	$^{+6.7}_{-6.4}$	$^{+5.1}_{-5.1}$	$^{+4.3}_{-3.8}$
530	0.032	1.28	± 7.6	$^{+6.5}_{-6.7}$	$^{+5.5}_{-5.5}$	$^{+3.4}_{-3.7}$
530	0.068	1.04	± 9.6	$^{+4.3}_{-3.4}$	$^{+1.8}_{-1.8}$	$^{+3.9}_{-2.9}$
530	0.13	1.11	± 11.1	$^{+3.3}_{-4.3}$	$^{+1.6}_{-1.6}$	$^{+2.9}_{-4.0}$
950	0.015	1.14	± 8.7	$^{+6.9}_{-7.5}$	$^{+6.2}_{-6.2}$	$^{+3.1}_{-4.2}$
950	0.032	1.15	± 6.3	$^{+6.7}_{-6.7}$	$^{+6.0}_{-6.0}$	$^{+2.9}_{-3.1}$
950	0.068	0.92	± 7.4	$^{+4.5}_{-4.5}$	$^{+3.6}_{-3.6}$	$^{+2.8}_{-2.7}$
950	0.13	0.88	± 8.8	$^{+3.1}_{-3.9}$	$^{+2.6}_{-2.6}$	$^{+1.7}_{-2.8}$
950	0.24	0.68	± 12.4	$^{+3.7}_{-3.1}$	$^{+2.5}_{-3.1}$	$^{+1.7}_{+1.0}$
1700	0.032	1.00	± 6.0	$^{+6.1}_{-6.1}$	$^{+5.8}_{-5.8}$	$^{+1.8}_{-1.7}$
1700	0.068	0.94	± 5.8	$^{+4.1}_{-3.9}$	$^{+3.7}_{-3.7}$	$^{+1.7}_{-1.1}$
1700	0.13	0.82	± 7.7	$^{+3.7}_{-3.1}$	$^{+2.5}_{-2.5}$	$^{+2.8}_{-1.8}$
1700	0.24	0.68	± 8.0	$^{+2.5}_{-2.7}$	$^{+2.5}_{-2.4}$	$^{-0.3}_{-0.9}$
1700	0.42	0.41	± 16.4	$^{+5.2}_{-4.8}$	$^{+4.4}_{-4.4}$	$^{-2.0}_{+2.8}$
3000	0.032	0.96	± 8.7	$^{+7.2}_{-6.9}$	$^{+6.7}_{-6.7}$	$^{+2.5}_{-1.7}$
3000	0.068	0.84	± 5.4	$^{+4.0}_{-4.1}$	$^{+4.0}_{-4.0}$	$^{+0.0}_{-0.6}$
3000	0.13	0.72	± 7.0	$^{+4.7}_{-4.6}$	$^{+4.6}_{-4.6}$	$^{+0.2}_{+0.6}$
3000	0.24	0.68	± 6.9	$^{+2.3}_{-2.5}$	$^{+2.3}_{-2.3}$	$^{-0.9}_{+0.5}$
3000	0.42	0.33	± 10.7	$^{+6.7}_{-5.1}$	$^{+4.3}_{-4.3}$	$^{-2.8}_{+5.2}$
5300	0.068	0.80	± 6.6	$^{+5.1}_{-4.8}$	$^{+4.7}_{-4.7}$	$^{-1.0}_{+2.0}$
5300	0.13	0.59	± 7.0	$^{+6.3}_{-6.3}$	$^{+6.2}_{-6.2}$	$^{-0.8}_{+1.3}$
5300	0.24	0.55	± 7.6	$^{+5.1}_{-5.1}$	$^{+4.4}_{-4.4}$	$^{-2.6}_{+2.6}$
5300	0.42	0.30	± 10.0	$^{+7.1}_{-7.5}$	$^{+4.8}_{-4.8}$	$^{-5.7}_{+5.2}$
5300	0.65	0.11	± 27.3	$^{+24.1}_{-25.1}$	$^{+20.5}_{-20.5}$	$^{-14.5}_{+12.7}$
9500	0.13	0.81	± 6.9	$^{+8.6}_{-8.8}$	$^{+7.5}_{-7.5}$	$^{-4.6}_{+4.1}$
9500	0.24	0.53	± 8.1	$^{+11.1}_{-10.2}$	$^{+9.4}_{-9.4}$	$^{-3.9}_{+5.8}$
9500	0.42	0.26	± 11.3	$^{+10.4}_{-9.6}$	$^{+6.6}_{-6.6}$	$^{-7.0}_{+8.1}$
9500	0.65	0.03	$^{+67.8}_{-43.4}$	$^{+30.5}_{-26.2}$	$^{+21.0}_{-21.0}$	$^{-15.7}_{+22.1}$
17000	0.24	0.52	± 9.3	$^{+14.0}_{-12.6}$	$^{+8.5}_{-8.5}$	$^{-9.3}_{+11.1}$
17000	0.42	0.20	± 14.5	$^{+16.6}_{-13.8}$	$^{+9.6}_{-9.6}$	$^{-9.8}_{+13.5}$
17000	0.65	0.05	$^{+54.1}_{-37.2}$	$^{+31.6}_{-28.9}$	$^{+20.6}_{-20.6}$	$^{-20.3}_{+23.9}$
30000	0.42	0.26	± 15.5	$^{+32.4}_{-27.8}$	$^{+19.8}_{-19.8}$	$^{-19.5}_{+25.7}$
30000	0.65	0.05	$^{+50.1}_{-35.2}$	$^{+52.5}_{-40.8}$	$^{+27.7}_{-27.7}$	$^{-30.0}_{+44.6}$

Table 7: *Values of the reduced cross section for $P_e = -0.27 \pm 0.01$. The following quantities are given: the values of Q^2 and x at which the cross section is quoted; the measured cross section; the statistical uncertainty; the total systematic uncertainty; the uncorrelated systematic uncertainty and the calorimeter energy-scale uncertainty (δ_{es}), which has significant correlations between cross-section bins.*

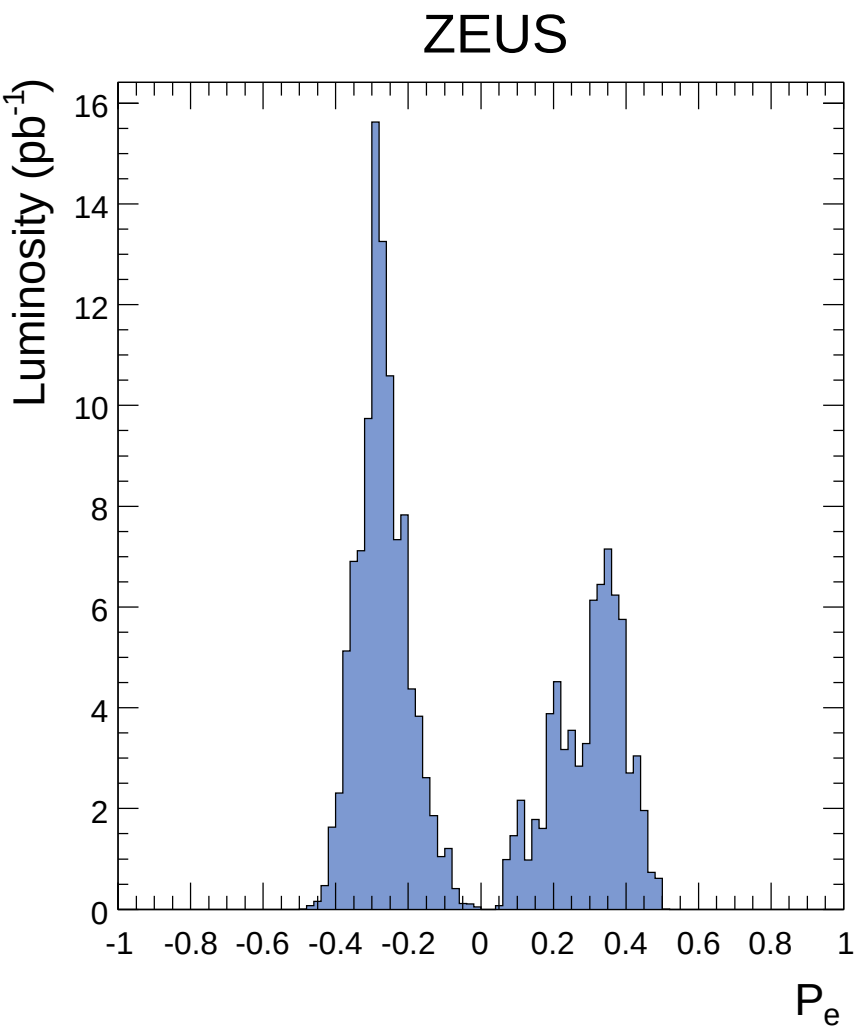

Figure 1: *The integrated luminosity collected as a function of the longitudinal polarisation of the electron beam.*

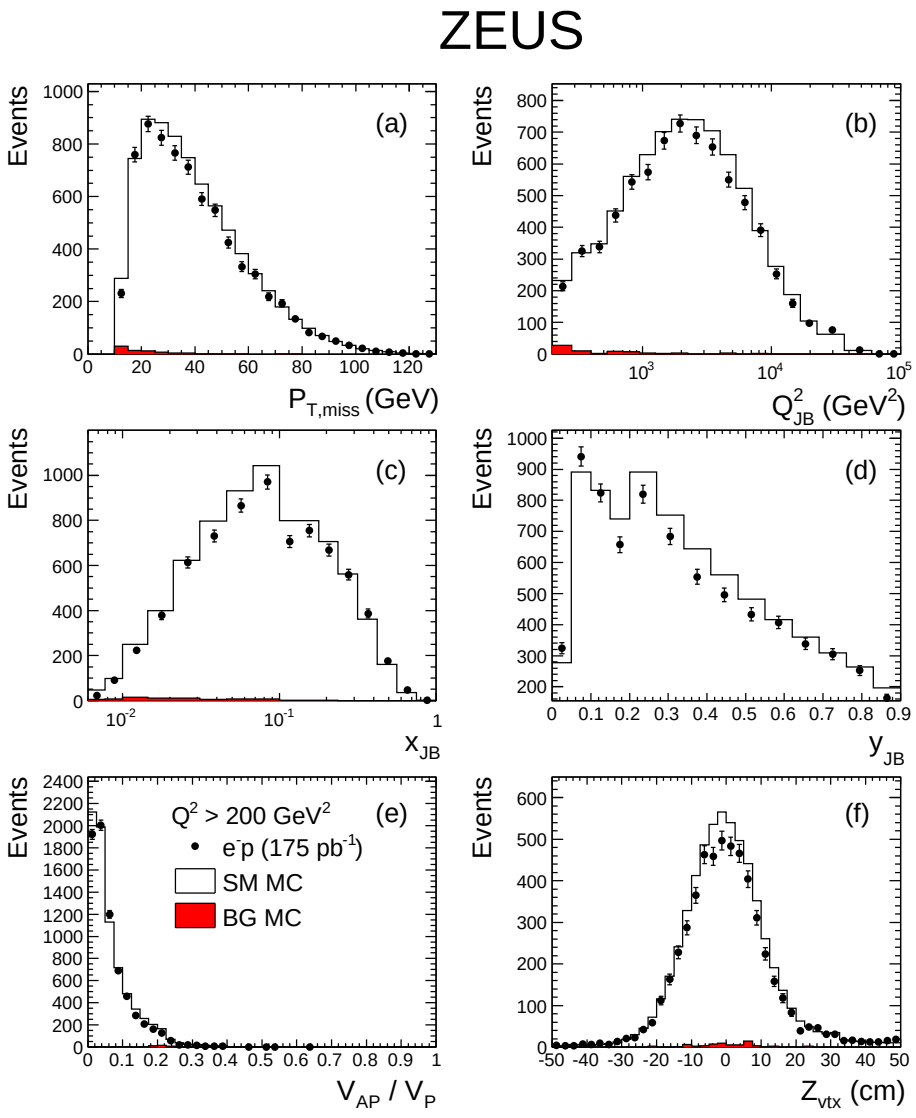

Figure 2: *Comparison of the e^-p CC data sample with the expectations of the MC simulation as described in Section 4 of the text. The distributions of (a) $P_{T,\mathrm{miss}}$, (b) Q^2_{JB}, (c) x_{JB}, (d) y_{JB}, (e) V_{AP}/V_P and (f) Z_{vtx} are shown.*

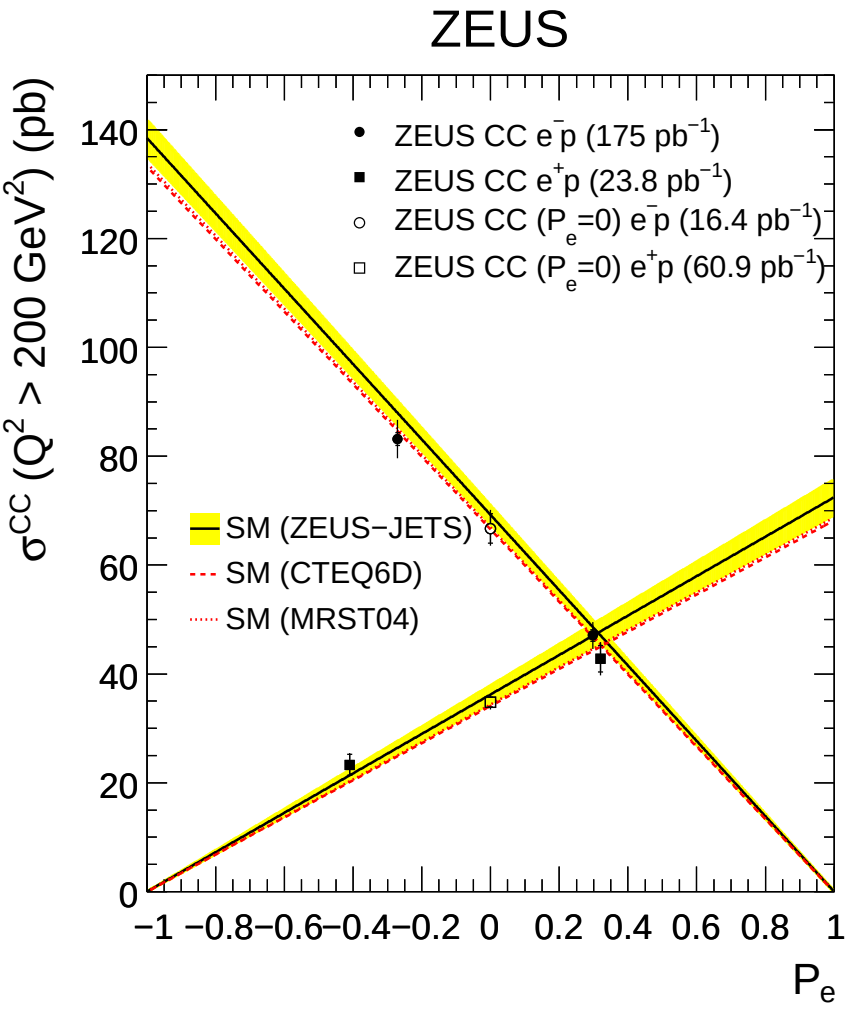

Figure 3: *The total cross sections for e^-p and e^+p CC DIS as a function of the longitudinal polarisation of the lepton beam. The lines show the predictions of the SM evaluated using the ZEUS-JETS, CTEQ6D and MRST04 PDFs. The shaded bands show the experimental uncertainty from the ZEUS-JETS fit.*

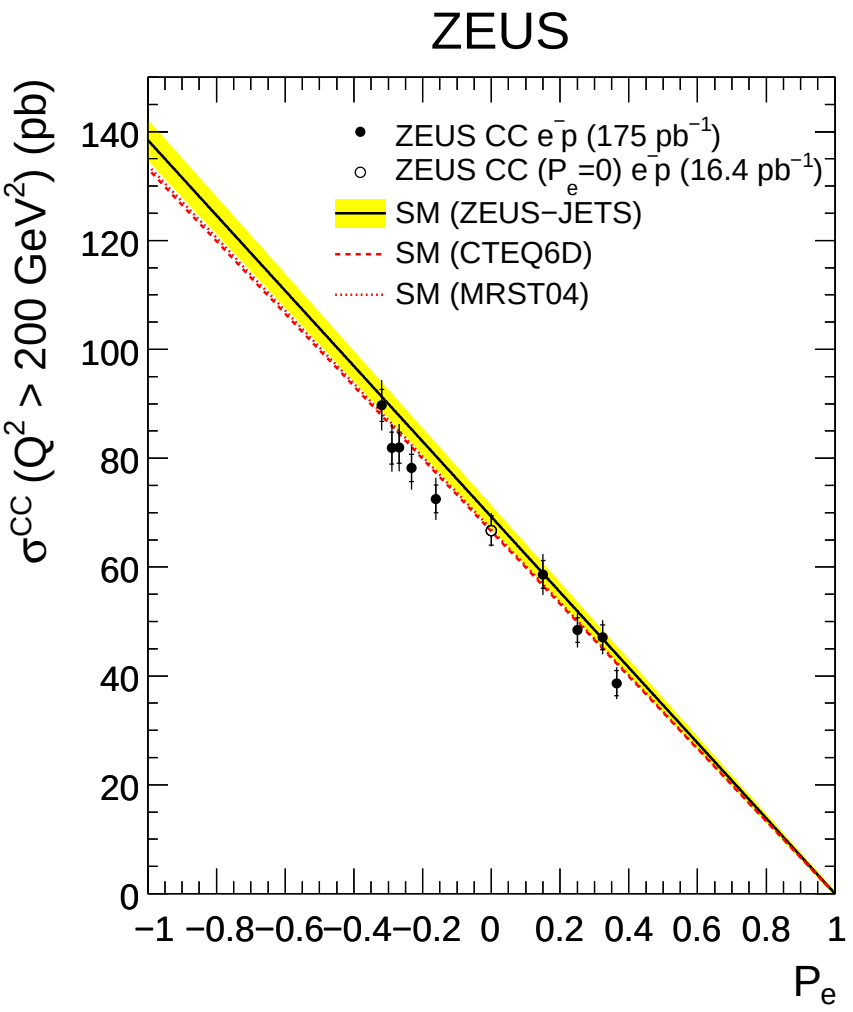

Figure 4: *The total cross sections for e^-p CC DIS as a function of the longitudinal polarisation of the electron beam. The lines show the predictions of the SM evaluated using the ZEUS-JETS, CTEQ6D and MRST04 PDFs. The shaded band shows the experimental uncertainty from the ZEUS-JETS fit.*

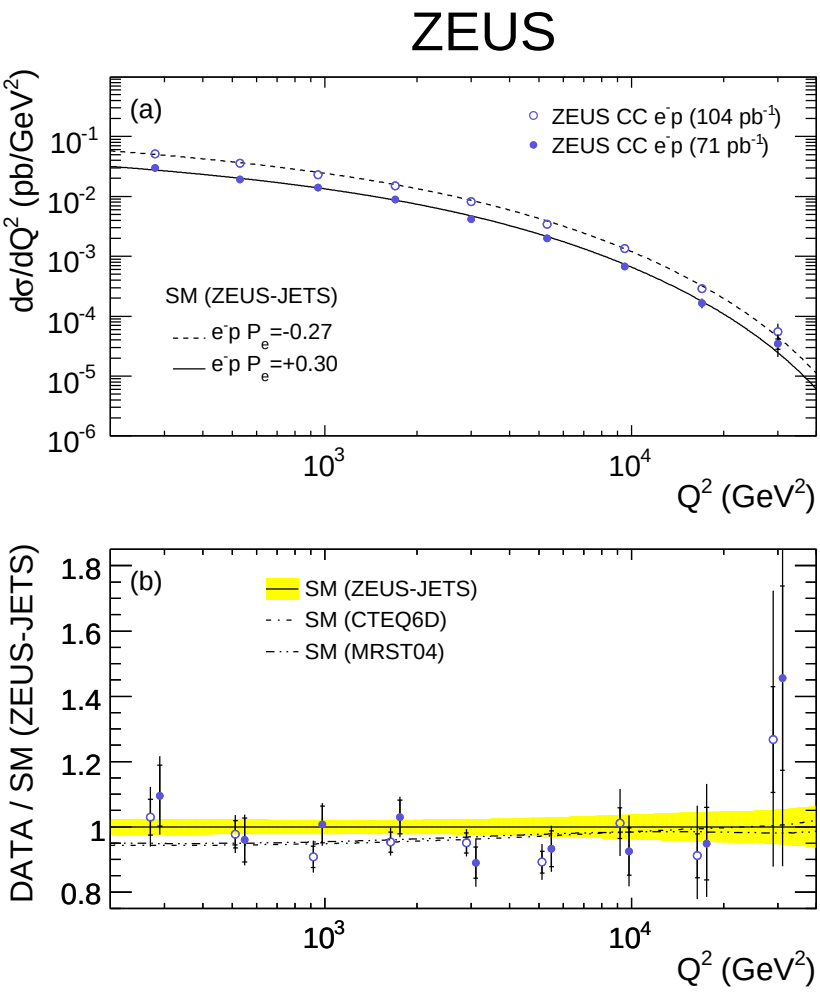

Figure 5: *(a) The e^-p CC DIS cross-section $d\sigma/dQ^2$ for data and the Standard Model expectation evaluated using the ZEUS-JETS PDFs. The postive (negative) polarisation data are shown as the filled (open) points, the statistical uncertanties are indicated by the inner error bars (delimited by horizontal lines) and the full error bars show the total uncertainty obtained by adding the statistical and systematic contributions in quadrature. (b) The ratio of the measured cross section, $d\sigma/dQ^2$, to the Standard Model expectation evaluated using the ZEUS-JETS fit. The shaded band shows the experimental uncertainty from the ZEUS-JETS fit.*

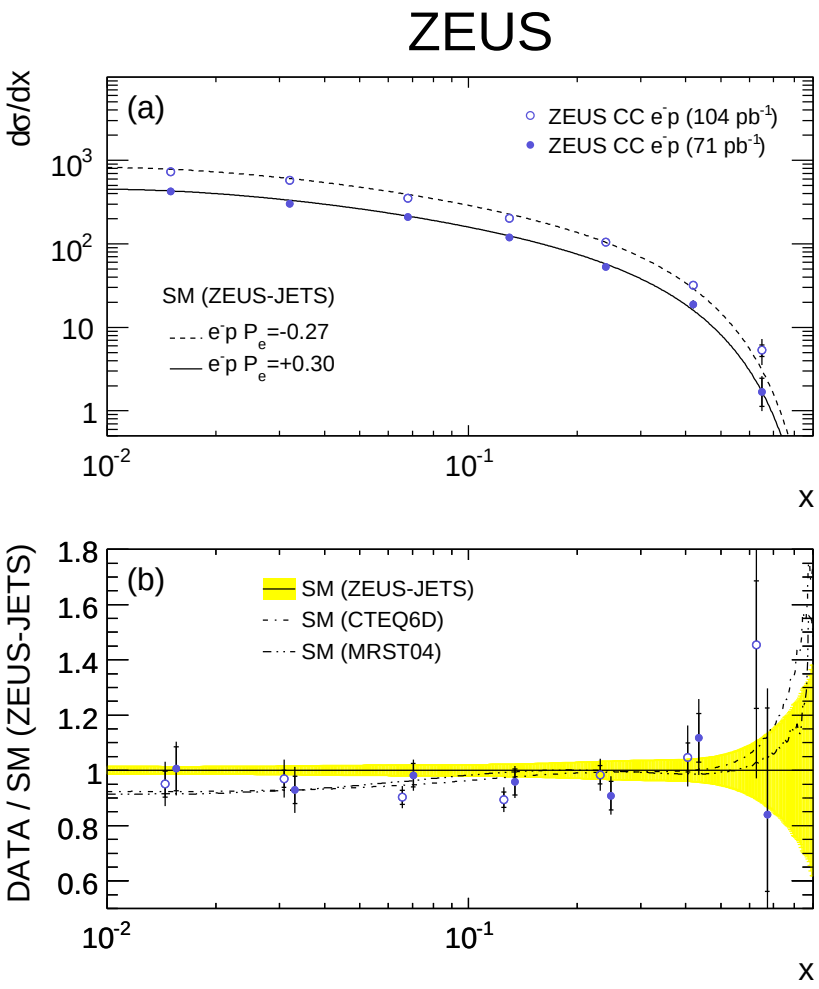

Figure 6: *(a) The e^-p CC DIS cross-section $d\sigma/dx$ for data and the Standard Model expectation evaluated using the ZEUS-JETS PDFs. The postive (negative) polarisation data are shown as the filled (open) points, the statistical uncertanties are indicated by the inner error bars (delimited by horizontal lines) and the full error bars show the total uncertainty obtained by adding the statistical and systematic contributions in quadrature. (b) The ratio of the measured cross section, $d\sigma/dx$, to the Standard Model expectation evaluated using the ZEUS-JETS fit. The shaded band shows the experimental uncertainty from the ZEUS-JETS fit.*

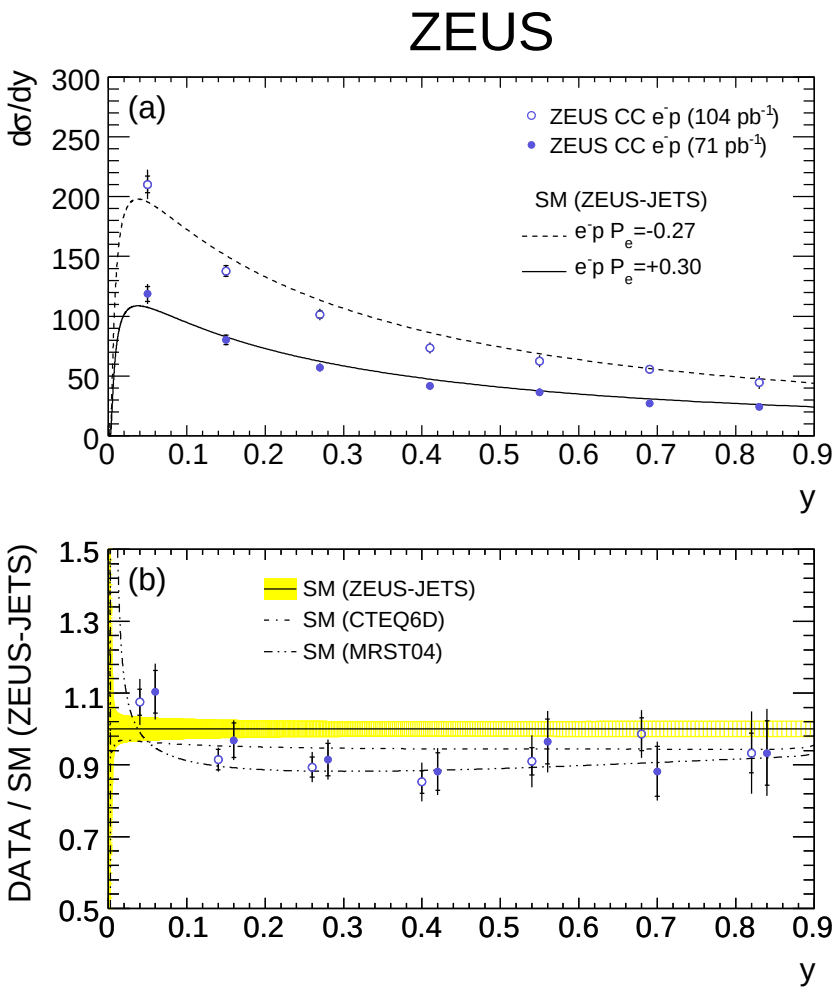

Figure 7: *(a) The e^-p CC DIS cross-section $d\sigma/dy$ for data and the Standard Model expectation evaluated using the ZEUS-JETS PDFs. The postive (negative) polarisation data are shown as the filled (open) points, the statistical uncertanties are indicated by the inner error bars (delimited by horizontal lines) and the full error bars show the total uncertainty obtained by adding the statistical and systematic contributions in quadrature. (b) The ratio of the measured cross section, $d\sigma/dy$, to the Standard Model expectation evaluated using the ZEUS-JETS fit. The shaded band shows the experimental uncertainty from the ZEUS-JETS fit.*

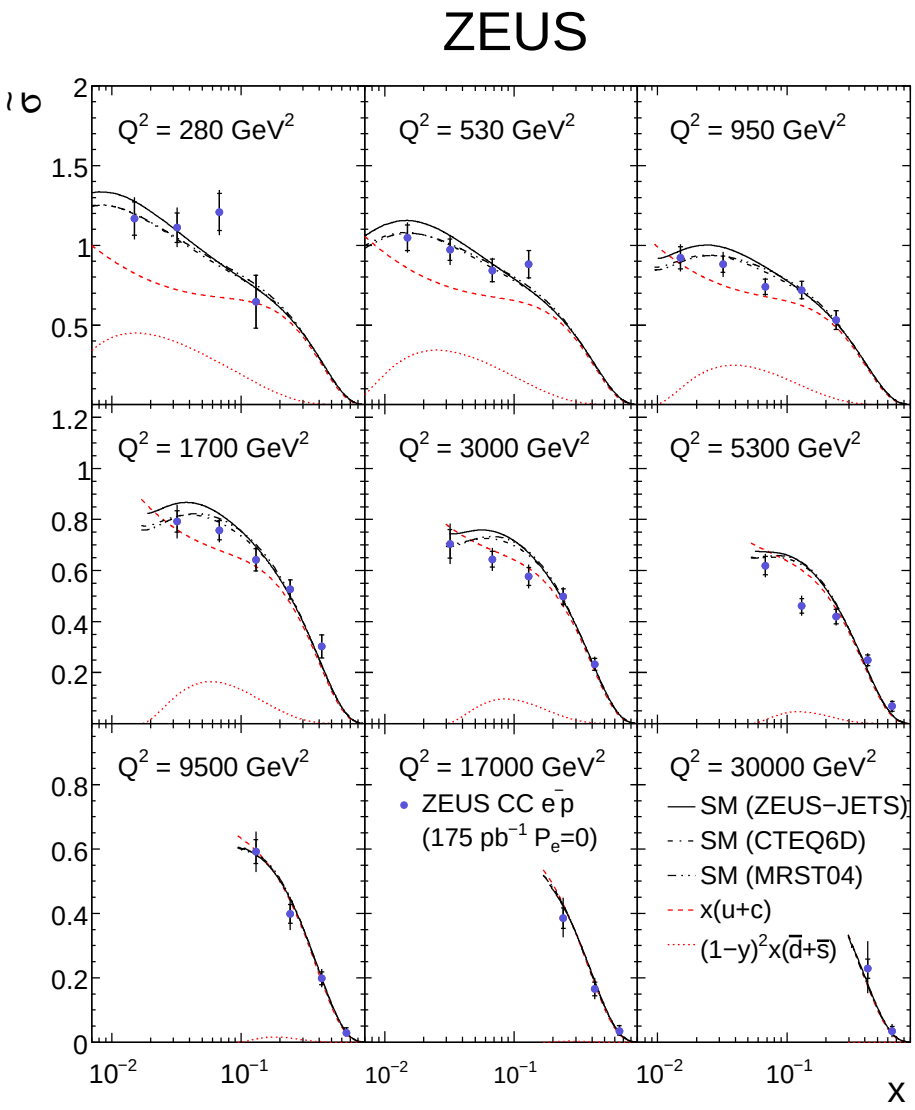

Figure 8: *The e^-p CC DIS reduced cross section plotted as a function of x for fixed Q^2. The circles represent the data points and the curves show the predictions of the SM evaluated using the ZEUS-JETS, CTEQ6D and MRST04 PDFs. The dashed and dotted lines show the contributions of the PDF combinations $x(u+c)$ and $(1-y)^2x(\bar{d}+\bar{s})$, respectively.*

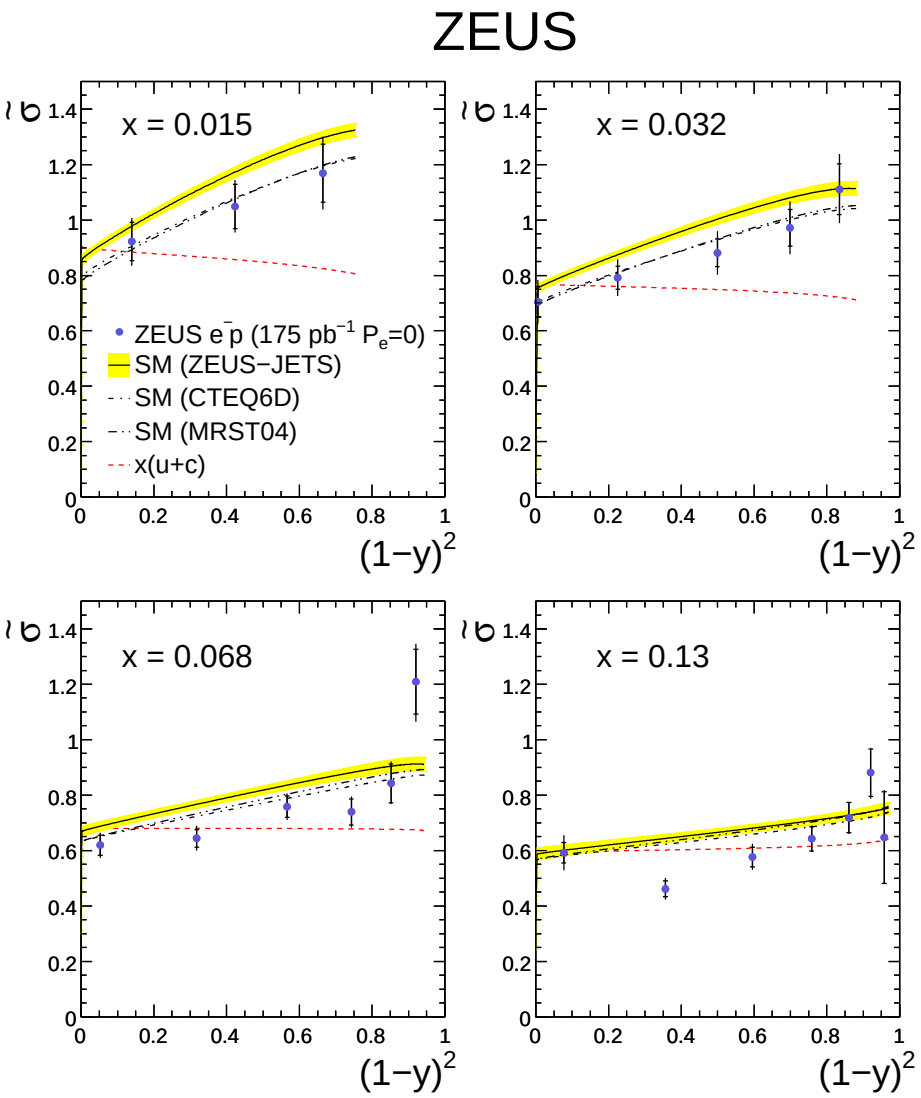

Figure 9: *The e^-p CC DIS reduced cross section plotted as a function of $(1-y)^2$ for fixed x. The circles represent the data points and the curves show the predictions of the SM evaluated using the ZEUS-JETS, CTEQ6D and MRST04 PDFs. The dashed lines show the contributions of the PDF combination $x(u+c)$ and the shaded band shows the experimental uncertainty from the ZEUS-JETS fit.*